

# **EQUIVALENT FRESHWATER MODELS FOR COASTAL AQUIFERS**

by

Shahynaz Sayed Abdel-Mohsen

A thesis submitted to the Department of Civil Engineering  
In conformity with the requirements for  
the degree of Master of Applied Science

Royal Military College of Canada

Kingston, Ontario, Canada

(April, 2014)

Copyright ©Shahynaz Sayed Abdel-Mohsen, 2014

## Abstract

The aim of this study was to investigate the impact of saltwater intrusion on the transient hydraulic behavior of coastal aquifers and to develop an Equivalent Freshwater Modeling (EFM) approach. The EFM approach proposed here focuses on the use of an Equivalent Freshwater Hydraulic Conductivity.

A two dimensional finite difference saltwater/freshwater model was developed using SEAWAT. An equivalent two dimensional freshwater-only model was also developed using MODFLOW. Both saltwater/freshwater and freshwater-only models were run under different recharge and pumping conditions. A comparison between the two models' behaviour was held to identify possible relationships between the hydraulic conductivity ( $K_s$ ) of the saltwater/freshwater model and the hydraulic conductivity ( $K_f$ ) of the freshwater-only model. For each value of  $K_s$  a calibration exercise was performed to choose the equivalent  $K_f$  value that gives the minimum Root Mean Square Error between the two models. Plots of the relationship between  $K_s$  and the optimal  $K_f$  values were generated for a range of  $K_s$  values and for a range of pumping conditions represented by the ratio of pumping rate over the freshwater lens thickness, ( $Q/B_f$ ). The optimal  $K_f$  values were then tested with three dimensional models.

From the different simulation scenarios we found that the presence of saltwater intrusion does not significantly affect the behavior of fine sand aquifers ( $K_s < 5$  m/d), under the full range of pumping and freshwater lens thicknesses considered in this study. In medium sand aquifers ( $10 < K_s < 25$  m/day), the presence of the intrusion requires an

Equivalent Freshwater Hydraulic Conductivity ( $K_f$ ) that is 20 to 30% higher than the original value, but the required  $K_f$  is fairly independent of the pumping over the freshwater lens thickness ratio ( $Q/B_f$ ). In coarse sand aquifers ( $K_s > 45$  m/day), the saltwater presence does have a significant effect on the aquifer behavior and the ratio of  $K_f$  over  $K_s$  is significantly affected by the freshwater lens thickness and the pumping rate. The 3-D model verifications, that were performed with Fine Sand and Medium Sand Hydraulic Conductivities only, confirmed the  $K_f/K_s$  relationships that were developed with the 2-D models. Finally, it was noted that the performance of the EFM approach was found to depend on the aquifer hydraulic conductivity, the freshwater lens thickness and the intensity of the pumping applied to the models.

## Résumé

Le but de cette étude était d'investiguer l'impact des intrusions salines sur le comportement hydraulique transitoire des aquifères côtiers et de développer une approche de Modélisation Équivalente d'Eaux Douces (MEED). L'approche MEED proposée ici, est axée sur l'utilisation d'une Conductivité Hydraulique d'Eau Douce Équivalente.

Un modèle bidimensionnel eaux salines / eaux fraîches en différence finies a été développé à l'aide de SEAWAT. Un modèle bidimensionnel eaux fraîches équivalent a aussi été développé avec MODFLOW. Les deux modèles ont été exécutés sous différentes conditions de recharge et de pompage. Une comparaison entre les deux modèles a été effectuée pour identifier les relations possibles entre la conductivité hydraulique ( $K_s$ ) du modèle eaux salines / eaux douces et la conductivité hydraulique ( $K_f$ ) du modèle eaux douces. Pour chaque valeur de  $K_s$  un exercice de calibration a été réalisé pour trouver le  $K_f$  équivalent qui minimise l'erreur-type entre les deux modèles. Des courbes de la relation entre  $K_s$  et les valeurs optimales de  $K_f$  ont été générées pour une gamme de valeurs de  $K_s$  et de conditions de pompages représentées par le rapport du taux de pompage sur l'épaisseur de la lentille d'eau fraîche ( $Q/B_f$ ). Les valeurs optimales de  $K_f$  ont été par la suite mises à l'essai avec des modèles tridimensionnels.

Des différents scénarios de simulation, on a noté que la présence d'une intrusion saline n'affecte pas de façon significative le comportement des aquifères de sable fin ( $K_s < 5$  m/d), pour la pleine gamme des taux de pompage et d'épaisseurs de lentille d'eau fraîche considérées dans cette étude. Dans les aquifères de sable moyen ( $10 < K_s < 25$  m/d), la présence d'une intrusion requière une conductivité hydraulique équivalente d'eau fraîche ( $K_f$ ) qui est de 20 à 30% plus élevée que la valeur originale, mais le  $K_f$  requis est plutôt

indépendant du rapport du pompage sur l'épaisseur de la lentille ( $Q/B_f$ ). Dans les aquifères de sable grossier ( $K_s > 45$  m/d), la présence de l'intrusion saline a un effet significatif sur le comportement de l'aquifère et le rapport de  $K_f$  sur  $K_s$  est appréciablement affecté par l'épaisseur de la lentille d'eau fraîche et le débit de pompage. Les vérifications avec le modèle tridimensionnel, qui ont été réalisées pour les sables fins et moyens seulement, ont confirmé les relations  $K_f/K_s$  qui ont été développées avec les modèles bidimensionnels. Finalement, on a observé que le rendement de l'approche MEED dépend de la conductivité hydraulique de l'aquifère, l'épaisseur de la lentille d'eau fraîche et l'intensité du pompage imposé aux modèles.

## **Acknowledgements**

Thank you God for helping, guiding and giving me the endurance to accomplish this work.

I would like to express my gratitude to my supervisor Dr. Michel Tétreault and my co-supervisor Dr. Micheal Hulley for their valuable help, guidance and encouragement throughout my research.

Many thanks to all professors, colleagues and staff members in the Civil Engineering Department at RMCC, especially Dr. Nicholas Vlachopoulos and Mrs. Majda El-Jaat.

I am deeply grateful to my small family, my husband Ahmed for his support and patience during my studies and to my little one Malek whose laughs and hugs made me stronger.

Great thanks to my lovely family (my father, mother, sisters, and my brother) for their support and prayers to encourage me to continue.

Finally, I miss my lovely grandfather who passed away during my research and was always looking forward to my graduation, may God cover him with his mercy.

# Table of Contents

Abstract.....	ii
Résumé.....	iv
Acknowledgements.....	vi
Table of Contents.....	vii
List of Tables .....	xiii
List of Symbols .....	xiv
List of Abbreviations .....	xvi
Chapter 1 Introduction .....	1
1.1 General.....	1
1.2 Saltwater Intrusion.....	2
1.3 Thesis Objectives .....	2
Chapter 2 Literature Review .....	4
2.1 Introduction.....	4
2.2 Properties of Saltwater.....	5
2.3 Saltwater/Freshwater Equilibrium .....	6
2.4 Types of Saltwater/Freshwater Interfaces.....	7
2.5 Analytical Solutions for Lateral Intrusion Problems .....	8
2.6 Analytical Solutions for Up-Coning Problems .....	9
2.7 Numerical Models.....	11
2.7.1 Finite Difference Codes .....	12
<b>2.7.1.1</b> SWIP .....	12
<b>2.7.1.2</b> VS2DT .....	12
<b>2.7.1.3</b> FTWORK.....	13
<b>2.7.1.4</b> SEAWAT .....	13
<b>2.7.1.5</b> MOCDENSE.....	13
2.7.2 Finite Element Codes .....	14
<b>2.7.2.1</b> SUTRA .....	14
<b>2.7.2.2</b> FEFLOW.....	15
<b>2.7.2.3</b> CODESA3D.....	15

2.7.2.4 FEMWASTE.....	15
2.7.2.5 FEMWATER .....	16
2.7.3 Code Selection .....	16
2.8 Summary .....	16
Chapter 3 SEAWAT and Henry’s Problem .....	17
3.1 Introduction.....	17
3.2 Development of SEAWAT .....	18
3.3 SEAWAT Mathematical Description and Development of Governing Equations.....	19
3.3.1 SEAWAT Basic Assumptions .....	19
3.3.2 Equivalent Freshwater Head Equations .....	19
3.3.3 Relationship Between $\rho$ and C .....	21
3.4 SEAWAT Governing Equations.....	21
3.5 SEAWAT Discretization Methods .....	24
3.5.1 Spatial Discretization Scheme .....	24
3.5.2 Temporal Discretization Scheme .....	24
3.6 Flow and Transport Coupling .....	25
3.6.1 Explicit Coupling of Flow and Transport .....	26
3.6.2 Implicit Coupling of Flow and Transport .....	27
3.7 SEAWAT Benchmark Problems .....	29
3.7.1 Box Problems.....	29
3.7.2 Elder’s Problem .....	30
3.7.3 HYDROCOIN Problem .....	30
3.7.4 Henry’s Problem .....	30
3.8 Testing Against Henry’s Problem.....	31
3.8.1 Model Formulation and Description .....	31
3.8.2 Finite Difference Grid Description .....	31
3.8.3 Boundary Conditions and Model Implementation.....	32
3.8.4 Results and Comparison .....	35
Chapter 4 Coastal Aquifer Model Description and Verification .....	36
4.1 General Purpose and Scope .....	36
4.2 Saltwater Model Formulation and Description.....	37
4.2.1 Model Area and Mesh Description .....	37
4.2.2 Model Hydrological Parameters .....	37



4.2.3 Model Boundary Conditions.....	38
4.2.4 Model Numerical Flow and Transport Solution Approach.....	38
4.3 Model Verification.....	40
4.3.1 Steady State Verification .....	41
4.3.2 Transient Verification .....	42
4.4 Summary .....	43
Chapter 5 Development and Verification of Equivalent Freshwater Models .....	44
5.1 Introduction.....	44
5.2 2D Freshwater Model Investigation.....	45
5.2.1 Methodology .....	47
5.2.2 First Simulation Set.....	48
<b>5.2.2.1</b> Pumping Scenario (a).....	49
<b>5.2.2.2</b> Pumping Scenario (b).....	51
5.2.3 Second Simulation Set .....	53
5.3 Compilation and Analysis of Results.....	54
Chapter 6 Verification with Three-Dimensional Models .....	60
6.1 Introduction.....	60
6.2 Three Dimensional Saltwater Model Description.....	60
6.2.1 Model Grid Description .....	60
<b>Figure 6-1 3D model dimensions</b> .....	61
6.2.2 Model Hydrogeological Parameters.....	61
6.2.3 Model Boundary Conditions.....	62
6.2.4 Model Numerical Flow and Transport Parameters .....	63
6.2.5 3D Freshwater Model Description.....	66
6.3 Simulations and Pumping Sets for R=0.005 m/d.....	66
6.3.1 First Pumping Set.....	66
6.3.2 Second Pumping Set .....	69
6.3.3 Third Pumping Set.....	72
6.4 Summary .....	75
Chapter 7 Conclusions and Recommendations.....	77
7.1 General.....	77
7.2 Conclusions.....	78
7.3 Recommendations and Future Work.....	79

**References..... 80**

## List of Figures

Figure 2-1 Saltwater intrusion phenomenon (Larabi, 2001).....	5
Figure 2-2 The hydrostatic balance between freshwater and saltwater by U-tube (Todd and Mays, 2011).....	6
Figure 2-3 Zone of transition between saltwater and freshwater (Reilly and Goodman, 1985) .....	8
Figure 2-4 Saltwater up-coning beneath well (Todd and Mays, 2011).....	10
Figure 3-1 Equivalent freshwater head (SEAWAT Guide, 2002) .....	20
Figure 3-2 Representitive Elementry Volume in porous medium (SEAWAT Guide, 2002) .	22
Figure 3-3 Explicit scheme for coupling in SEAWAT (SEAWAT Guide, 2002).....	27
Figure 3-4 Implicit coupling approach scheme (SEAWAT Guide, 2002) .....	28
Figure 3-5 Henry’s problem model parameters (SEAWAT Guid, 2002) .....	31
Figure 3-6 Henry’s problem finite-difference grid .....	32
Figure 3-7 Henry’s problem concentration distributions.....	33
Figure 3-8 Comparison between published Henry’s problem solution and SEAWAT solution to the Henry’s problem .....	35
Figure 4-1 Model dimensions .....	37
Figure 4-2 2D saltwater/freshwater generic aquifer model.....	39
Figure 4-3 Illustration the selected columns.....	41
Figure 4-4 Model output showing up-coning during pumping .....	43
Figure 5-1 Equivalent freshwater head distribution at constant –head boundaries.....	47
Figure 5-2 Water table response comparison for (a) pumping scenario when $K_s = 5 \text{ m/day}$ .....	50
Figure 5-3 Water table response comparison for (a) pumping scenario when $K_s = 10 \text{ m/day}$ .....	51
Figure 5-4 Water table response comparison for (b) pumping scenario when $K_s = 15 \text{ m/day}$ .....	52
Figure 5-5 Water table response comparison for (b) pumping scenario when $K_s = 20 \text{ m/day}$ .....	53
Figure 5-6 General trend of the relationship between $K_s$ and $K_f$ for $R=0.005 \text{ m/day}$ .....	55
Figure 5-7 General trend of the relationship between $K_s$ and $K_f$ for $R=0.008 \text{ m/d}$ .....	56
Figure 5-8 Summary of the relationship between $Q/B_f$ and RMSE for $B_f = 50 \text{ m}$ .....	57
Figure 5-9 Summary of the relationship between $Q/B_f$ and RMSE for $B_f = 70 \text{ m}$ .....	57

<b>Figure 5-10 Difference in head distribution for the first pumping scenario for <math>K_s = 5</math> m/day and <math>K_f = 5.5</math> m/day .....</b>	<b>58</b>
<b>Figure 5-11 Difference in head distribution for the second pumping scenario for <math>K_s = 5</math> m/day and <math>K_f = 5.5</math> m/day.....</b>	<b>59</b>
<b>Figure 5-12 Difference in head distribution for the third pumping scenario for <math>K_s = 5</math> m/day and <math>K_f = 5.5</math> m/day .....</b>	<b>59</b>
<b>Figure 6-1 3D model dimensions .....</b>	<b>61</b>
<b>Figure 6-2 Locations of pumping and monitoring wells.....</b>	<b>63</b>
<b>Figure 6-4 Head difference between <math>K_s</math> and <math>K_f</math> models for 3D- a' scenario.....</b>	<b>68</b>
<b>Figure 6-5 Head difference between <math>K_s</math> and <math>K_f</math> models for 3D- b' scenario .....</b>	<b>68</b>
<b>Figure 6-6 Head difference between <math>K_s</math> and <math>K_f</math> models for 3D- c' scenario.....</b>	<b>69</b>
<b>Figure 6-8 Head difference between <math>K_s</math> and <math>K_f</math> models for 3D- e' scenario.....</b>	<b>71</b>
<b>Figure 6-9 Head difference between <math>K_s</math> and <math>K_f</math> models for 3D- f' scenario .....</b>	<b>71</b>
<b>Figure 6-10 Head difference between <math>K_s</math> and <math>K_f</math> models for 3D- g' scenario.....</b>	<b>72</b>
<b>Figure 6-11 Head difference between <math>K_s</math> and <math>K_f</math> models for 3D- h' scenario .....</b>	<b>72</b>
<b>Figure 6-12 Head difference between <math>K_s</math> and <math>K_f</math> for 3D- i' scenario .....</b>	<b>74</b>
<b>Figure 6-13 Head difference between <math>K_s</math> and <math>K_f</math> for 3D- j' scenario .....</b>	<b>74</b>
<b>Figure 6-14 Head difference between <math>K_s</math> and <math>K_f</math> for 3D- k' scenario .....</b>	<b>75</b>
<b>Figure 6-15 Head difference between <math>K_s</math> and <math>K_f</math> for 3D- l' scenario.....</b>	<b>75</b>

## List of Tables

Table 2-1 Water type based on total dissolved solids (TDS) .....	5
Table 3-1 Input and Numerical solution parameters for the Henry's problem, (Langevin and Guo , 2006) .....	34
Table 4-1 Input and Numerical solution parameters for the saltwater generic aquifer model .....	40
Table 5-1 Representative hydraulic conductivity values for different sand soil types (Morris and Johnson, 1967) .....	45
Table 5-2 Input and Numerical solution parameters for the freshwater generic aquifer model .....	46
Table 5-3 Ratios of $Q/B_f$ for first simulation set .....	49
Table 5-5 Optimum $Kf$ value determination for $Ks= 10$ m/day .....	51
Table 5-6 Optimum $Kf$ value determination for $Ks= 15$ m/day .....	52
Table 5-7 Optimum $Kf$ value determination for $Ks = 20$ m/day .....	53
Table 5-8 Ratios of $Q/B_f$ for first simulation scenario .....	54
Table 6-1 Summary of types and positions of wells used in the 3D model .....	62
Table 6-2 Input and Numerical solution parameters for the saltwater generic aquifer model .....	65
Table 6-3 $Ks$ values for the 3D model in the first simulation set .....	67
Table 6-4 Comparison between RMSE for 2D and 3D models .....	67
Table 6-5 $Ks$ values for the 3D model in the first simulation set .....	70
Table 6-6 Comparison between RMSE for 2D and 3D model .....	70
Table 6-7 $Ks$ values for the 3D model in the first simulation set .....	73
Table 6-8 Comparison between RMSE for 2D and 3D model .....	73

## List of Symbols

A	Cross sectional area ( $m^2$ )
C	Solute concentration ( $kg/m^3$ )
$c_{ini}$	Initial concentration ( $kg/m^3$ )
$c_r$	Courant number
$D_d$	Effective diffusion coefficient ( $m^2/day$ )
$D_0$	Free solution diffusion
$D_m$	Molecular diffusion ( $m^2/day$ )
$D_h$	Hydrodynamic dispersion coefficient ( $m^2/day$ )
d	Distance from the initial position of the interface up to the bottom of the screen well ( $m$ )
G	Ratio between mass production/mass consumption
$h_f$	Freshwater rise( $m$ )
$h_s$	Saltwater rise ( $m$ )
$h_{ef}$	Equivalent freshwater head ( $m$ )
i	Hydraulic gradient
K	Hydraulic conductivity ( $m/day$ )
k	Soil permeability ( $m^2$ )
$K_f$	Freshwater hydraulic conductivity ( $m/day$ )
$K_s$	Saltwater hydraulic conductivity ( $m/day$ )
$K_d$	Retardation factor
n	Effective porosity
$P_N$	Pressure head at point N ( $N/m^2$ )
$Q_{max.}$	Maximum pumping rate ( $m^3/day$ )
q	Freshwater flow per unit length ( $m/day$ )

R	Recharge rate ( <i>m/day</i> )
$S_s$	Specific storage
$S_y$	Specific yield
t	Traveling time (day)
$v_i$	Groundwater velocity ( <i>m/day</i> )
v	Average liner velocity ( <i>m/day</i> )
$x_0$	Width of the submarine zone ( <i>m</i> )
$Z_{cr}$	Up-coning critical rise ( <i>m</i> )
$Z_N$	Elevation head at point N ( <i>m</i> )
$Z_{max.}$	Maximum rise of the interface ( <i>m</i> )
$\alpha_l$	Longitudinal dispersivity
$\Delta Z$	Observed up-coning ( <i>m</i> )
$\Delta\rho$	Difference in density between saltwater and freshwater ( <i>kg/m<sup>3</sup></i> )
$\mu$	Dynamic viscosity of saltwater ( <i>kg/m.s.</i> )
$\mu_f$	Dynamic viscosity of fresh water ( <i>kg/m.s.</i> )
$\theta$	Volumetric water content
$\rho_f$	Freshwater density ( <i>kg/m<sup>3</sup></i> )
$\rho_s$	Saltwater density ( <i>kg/m<sup>3</sup></i> )
$\tau$	Tortuosity coefficient

## List of Abbreviations

CHD	Constant Head Package.
FD	Finite Difference.
FE	Finite Element.
GCG	Generalized Conjugate Gradient.
PCG	Preconditioned Conjugate Gradient.
REV	Representative Elementary Volume.
RMSE	Root Mean Square Error.
TDS	Total Dissolved Solids.
TVD	Total Variation Diminishing.
2D	Two dimensional.
3D	Three dimensional.



# Chapter 1

## Introduction

### 1.1 General

Groundwater resources management requires maximizing water extraction in a sustainable fashion. In typical aquifers the process involves establishing water budgets, delineating wellhead protection areas and, sometimes, minimizing the impact of the withdrawals on the water table. These problems are usually analyzed with the help of groundwater models. These models can be quite complex and computationally intensive, depending on the scale, resolution and nature of the boundary conditions (Siarkos, and Latinopoulos, 2012).

In coastal areas, the impact of the withdrawals on the saline intrusion and conversely, the impact of the saline intrusion on the response (quantity and quality) of the aquifer must also be considered. Modeling a coastal aquifer encroached by a saline intrusion requires a code that can account for the effect of the density difference between freshwater and seawater and for the solute transport processes that control the salinity (and therefore the density). This requirement adds a very significant computational burden to any modeling effort and renders the use of saline intrusion models impractical for most groundwater management applications. A recent coastal aquifer modeling project (Tétreault and Hulley, 2011) gave rise to the idea that a freshwater-only model can perhaps effectively predict the behaviour of a coastal aquifer provided the aquifer parameters and boundary conditions are adjusted to account for the influence of the saline intrusion.

## **1.2 Saltwater Intrusion**

Saline water is one of the most common pollutants in fresh groundwater. All coastal aquifer zones are subjected to saline intrusion. The saltwater intrusion phenomenon occurs under natural undisturbed conditions due to the higher density of saltwater coming in from the ocean boundary. The intrusion can be exacerbated by rising sea levels and by freshwater extraction. Freshwater and saltwater are miscible fluids and therefore the zone of contact between them is affected by diffusion and dispersion processes. This leads to the presence of a transition zone between the two. In the analysis of saline intrusions, the interface between the freshwater and the saltwater is often treated, for simplification, as a “Sharp Interface” where the freshwater and saltwater are considered immiscible. This assumption is the basis of most analytical solutions and has been used in a number of numerical models. The assumption is considered reasonable when the thickness of the actual transition zone is small compared to the thickness of the aquifer (Reilly and Goodman, 1987), but this condition is difficult if not impossible to verify.

## **1.3 Thesis Objectives**

Modeling coastal aquifers is potentially considerably complicated by the presence of the saltwater intrusion. While the impact of the intrusion on the water quality is undeniable and very significant, the influence of the intrusion on the hydraulic response of the groundwater system is less obvious. The effect of fluid density gradients on the flow of groundwater is well understood and many groundwater modeling codes can account for it; however the process is computationally intensive and very sensitive to temporal and spatial discretization.

The issue of interest here is to study the effect of the presence of saltwater on the behavior of a coastal aquifer and to investigate the possibility of using an Equivalent Freshwater model that would be simpler to implement and use than a Saltwater/Freshwater model. The objectives of this thesis are:

- To develop a two dimensional saltwater/freshwater model of a generic coastal aquifer.
- To develop a two dimensional freshwater-only model of the same generic aquifer.
- To compare the behaviour of the freshwater component in both models and identify possible relationships that would support the development of equivalent modeling approaches. The focus at this time will be the relationship between the equivalent freshwater hydraulic conductivity  $K_f$  and the actual aquifer Hydraulic Conductivity  $K_S$ .
- To develop a three dimensional saltwater/freshwater model and a three dimensional freshwater model of a generic coastal aquifer.
- To apply the 2D Equivalent Freshwater Hydraulic Conductivity values to the 3D freshwater model and compare the response of this model to the response of the 3D Freshwater/Saltwater model.

## Chapter 2

### Literature Review

#### 2.1 Introduction

Saltwater intrusion is a natural process that occurs in all coastal aquifers. Saltwater intrusion can be defined as a movement of saltwater inland into fresh groundwater. Many factors influence saltwater intrusion such as, tidal effects, freshwater head fluctuations, and human activities such as pumping that produce saline water under the pumping well. Salinization of aquifers and wells is often a consequence of saltwater intrusion. Preventing this phenomenon is difficult so the aim is to control, rather than prevent it. Figure 2-1 shows a cross section of a saltwater intrusion interface for a homogeneous isotropic unconfined aquifer in hydrostatic equilibrium where  $z$  is the vertical distance from the mean sea level to the interface and  $h_f$ , is the freshwater thickness from the mean sea level to the phreatic surface.

This chapter consists of two sections. The first section presents a brief summary of the most common analytical methods that are used to determine the shape and position of the saline interface produced by lateral intrusion, the second section reviews the up-coning that arises due to pumping freshwater above a saline intrusion and the third section reviews the numerical models available to simulate saline intrusions.

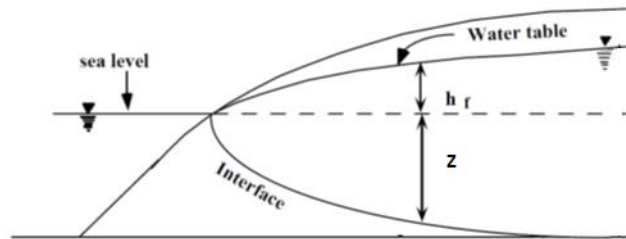


**Figure 2-1 Saltwater intrusion phenomenon (Larabi, 2001)**

## 2.2 Properties of Saltwater

The major factor in determining the movement of a saltwater wedge below the freshwater is the density, (Reilly and Goodman, 1985). The density range from fresh to saltwater has been classified into four groups by Krieger (1957). This classification was based on the total dissolved solids (TDS) in freshwater. Krieger found that at 20°C, the density of pure freshwater is 0.9982 Kg/L and the density of brine saltwater is 1.345 Kg/L. From the Krieger classification, Chow, (1964) found that the average saltwater density range is between 1.022 and 1.028 Kg/L. This average density depends on temperature and solute concentration. Most researchers consider the average density of saltwater to be 1.025 kg/L. A general classification of salinity ranges is presented in Table 2-1 (Abd-Elhamid, 2011).

**Table 2-1 Water type based on total dissolved solids (TDS)**

TDS(mg/L)	Description
<1000	Fresh
1000-3000	Slightly saline
3000-10000	Moderately saline
10000-35000	Very saline
> 35000	Brine

## 2.3 Saltwater/Freshwater Equilibrium

Ghyben and Herzberg were the first to propose an explanation why saltwater in coastal aquifers was found at a depth below sea level of about 40 times the height of freshwater above sea level. They proposed a relationship based on the difference in densities between fluids. Figure 2-2 illustrates the hydrostatic balance between freshwater and saltwater in a U-tube (Todd and Mays, 2011).

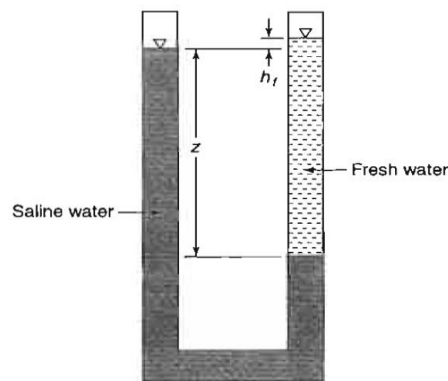


**Figure 2-2 The hydrostatic balance between freshwater and saltwater by U-tube (Todd and Mays, 2011)**

The Ghyben-Herzberg relationship is valid for unconfined aquifers and for confined aquifers, where the water table is replaced by the piezometric surface of the freshwater. Equations (1) and (2) and figure 2.2 illustrate the Ghyben-Herzberg relationship (Todd and Mays, 2011).

$$\rho_s g z = \rho_f g (z + h_f) \quad (1)$$

$$z = \frac{\rho_f}{(\rho_s - \rho_f)} h_f \approx 40 h_f \quad (2)$$

where;

$z$  : is the depth of the saltwater/freshwater interface below sea level.

$h_f$ : is the freshwater rise above sea level.

$\rho_s$  : saltwater density ( $\text{kg/m}^3$ ).

$\rho_f$ : freshwater density ( $\text{kg/m}^3$ ).

## **2.4 Types of Saltwater/Freshwater Interfaces**

In the relatively homogeneous porous media in a coastal area Cooper (1964) has found that denser saltwater tends to stay separated from the overlying freshwater; however there is a transition zone between dense saltwater and freshwater. Two types of zones between salt and freshwater can developed; sharp interface and transition zone. The interface is considered to be sharp when the thickness of the zone between saltwater and freshwater is less than 1/3 of the freshwater thickness. In sharp interface situations, saltwater and freshwater are normally treated as immiscible fluids. In the transition zone freshwater and saltwater are treated as miscible fluids and the concentration distribution is governed by the solute transport equation. Figure 2-3 illustrates the zone of diffusion between saltwater and freshwater in a homogeneous coastal aquifer (Reilly and Goodman, 1987).

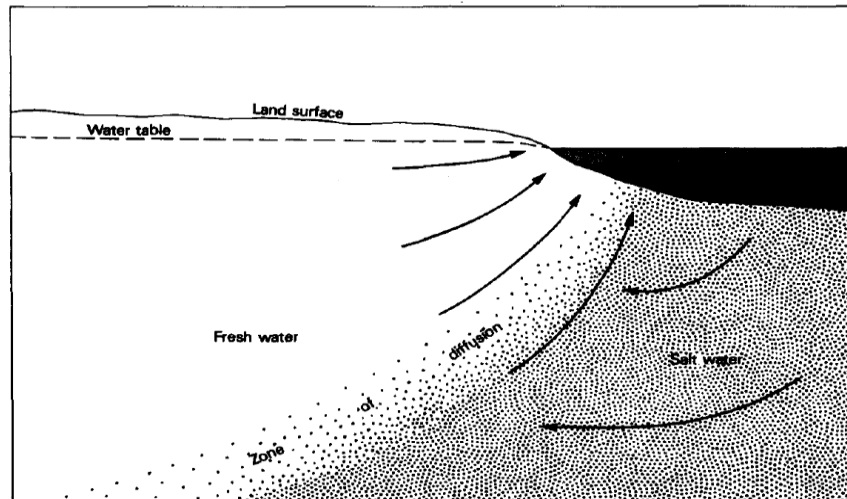


Figure 2-3 Zone of transition between saltwater and freshwater (Reilly and Goodman, 1985)

## 2.5 Analytical Solutions for Lateral Intrusion Problems

Over the past several decades, much research has been completed addressing the shape and position of the saltwater interface under various conditions. These methods first attempted to determine the effects of the dispersion and density dependent fluid flow in saltwater encroachment in coastal aquifers. The approach was to develop analytical equations for the interface problems in 2D and 3D. For the 2D problems some of these methods were based on Dupuit's assumption, which states that the equipotential in the flow system are perfectly vertical, which is reasonable when the slope of the phreatic surface is very small. In 1959, Henry developed several solutions to describe the characteristics of the sharp interface under various conditions. Cooper (1959) discussed a hypothesis concerning the dynamic balance of freshwater and saltwater in coastal aquifers. Henry in 1964 was the first to corroborate Cooper's hypothesis and treat the saltwater intrusion phenomenon as a solute transport issue based on the advection-diffusion equation. Henry (1964) also was the first to develop a



method to determine the effects of dispersion and density – dependent fluid flow on saltwater encroachment in costal aquifers. Henry in 1964 advanced Cooper’s hypothesis and accounted for hydrodynamic dispersion for miscible fluids, since Cooper’s theory only considered a sharp interface. The shape and position of the sharp interface have been calculated analytically by Cooper (1960), Glover (1959), Bear (1964), Van Der Veer (1977), Van Dam (1983) and Strack (1971) for homogeneous and isotropic aquifers.

A summary description of the methods presented above can be found in Abdel-Mohsen (2014). None of the methods above are useful for our objectives. It was hoped that an analytical solution could be used to validate our numerical model, but the required simplified conditions cannot be implemented in a numerical model.

## **2.6 Analytical Solutions for Up-Coning Problems**

Up-coning of saline water can occur in costal aquifers containing an underlying layer of saline water. When the freshwater lens is pumped by a partially penetrating well, the local interface below that well rises in response. This interface will be horizontal prior to pumping, however, once sustained pumping begins and the drawdown becomes sufficiently large, the saline interface rises progressively, as the freshwater level drops, until eventually it can reach the well. At that time the pumping has to be shut down as the saltwater can enter the well. When the pumping is stopped, the denser saline water will return to its former position in response to the recovery (rise) of the freshwater level, Figure 2-4 illustrates the up-coning phenomenon in a semi-confined aquifer, where;  $Q$ , is the pumping rate,  $r$ , is the pumping well radius,  $d$ , is the distance from the bottom of the well screen to the interface and  $Z$ ; is the critical rise.

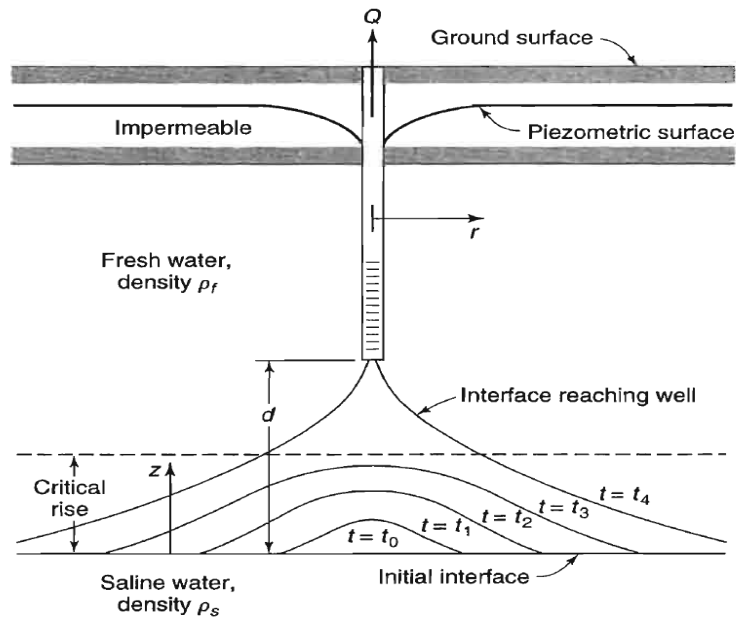


**Figure 2-4 Saltwater up-coning beneath well (Todd and Mays, 2011)**

Because up-coning is a very important phenomenon much research and studies have been done to determine the optimum location, depth, spacing, pumping rates and pumping sequence that will ensure the largest amount of freshwater and at the same time the minimum underground mixing between freshwater and saltwater. Most of the up-coning studies assume that the interface under the pumping well is sharp between fresh and saltwater. Although it is inaccurate to assume a sharp interface as it ignores the physical reality of the transition zone between both fluids, this assumption has the advantage of simplicity. The sharp interface can be considered as an approximation of the position of almost 50% relative salinity in a transition zone for sandy soils, (Tain *et.al.*, 1997).

Most analytical solutions that were proposed to calculate the up-coning critical rise ( $Z_{cr}$ ) and the maximum pumping rate ( $Q_{max}$ ) were assuming a sharp interface. The critical rise is

defined as an approximate estimated depth that follows the maximum permissible pumping rate before the saltwater enters the well. Most up-coning theories are based on Dupuit's assumptions, homogeneous and non-deformable soil, the two fluids are incompressible and separate and the flow obeys Darcy's law. From the Ghyben-Herzberg relation, Schmorak and Mercado (1969) proposed an approximate analytical solution for the up-coning directly beneath a well for a confined aquifer. A more detailed description of the methods presented above can be found in Abdel-Mohsen (2014). Similar to what was said in the previous section, none of the analytical solutions found could be used to validate our Saltwater/Freshwater models.

## **2.7 Numerical Models**

Numerical modeling is a useful and efficient tool for addressing groundwater problems. Groundwater models can be used in many areas such as; understanding why the flow system is behaving in a particular observed manner, or to predict how a flow system will behave in the future, to analyze a hypothetical flow situation in order to gain generic understanding of a particular flow system, to estimate the effect of contaminant injection and transport in space and time, and to predict the effect of groundwater stresses (groundwater recharge and discharge). Although the term model refers to a real system representation, the complexity of real systems can never be completely represented and simplifying assumptions are required.

In this section; a brief overview of the most common Finite Element and Finite Difference groundwater modeling codes will be presented, with the aim of selecting a code for our project. A more extensive review of groundwater and saltwater intrusion modelling can be found in Abdel-Mohsen (2014).

### **2.7.1 Finite Difference Codes**

The most common finite-difference codes capable of modelling a saline intrusion are:

- SWIP (SWENT and SWIFT)
- VS2DT
- FTWORK
- SEAWAT
- MOCDENSE

#### **2.7.1.1 SWIP**

SWIP is considered the early general-purpose finite difference code for transport modeling. SWIP was developed by the U.S Geological Survey in (1976) to simulate three-dimensional heat and contaminant transport in anisotropic and heterogeneous porous media. New codes were developed and produced from SWIP to simulate and solve a coupled flow and solute transport and variable density conditions such as SWENT and SWIFT (Zheng and Bennett 2002).

#### **2.7.1.2 VS2DT**

VS2DT is a two dimensional finite difference code; developed by the U.S Geological Survey USGS in 1990. The code is able to simulate solute transport under variably saturated conditions. It is designed to work with the finite difference flow code VS2D which was developed by the USGS, (Zheng and Bennett 2002).

#### **2.7.1.3 FTWORK**

FTWORK is a three dimensional finite difference code developed in 1990 by Faust. FTWORK code simulates both flow and solute transport when the fluid density is constant, so the flow and transport equations are decoupled and independently solved. Because of this approach, FTWORK is computationally efficient. However, it can't be used for density or temperature –dependent transport problems, (Faust, 1990).

#### **2.7.1.4 SEAWAT**

SEWAT is a 3-D finite difference program that simulates variable-density transient groundwater flow in porous media. The source code for SEAWAT was developed by combining MODFLOW and MT3DMS into a single software to solve the coupled flow and solute transport equations. The SEAWAT code was tested by simulating five benchmark problems involving variable density groundwater flow. These problems include two box problems that were used to verify that fluid velocities are calculated properly by SEAWAT. The other three problems are; the Henry's problem, the Elder's problem and the HYDROCOIN problem. SEAWAT simulation results for the Henry's problem and the Elder's problem were almost the same as those obtained with SUTRA. For the HYDROCOIN problem SEAWAT gave almost the same results as those obtained with the MOCDENSE software, (USGS, 2002).

#### **2.7.1.5 MOCDENSE**

It is a two-dimensional finite-difference and particle-tracking model that simulates solute transport in flowing groundwater. It works for constant or variable density fluids. MOCDENSE was documented and released by Sanford and Konikow in 1985. MOCDENSE uses an implicit finite-difference approach to solve the flow system and a combination of

particle tracking and explicit finite difference to simulate the transport problem, (USGS, 1996).

### **2.7.2 Finite Element Codes**

The most common finite-element codes capable of modelling a saline intrusion are:

- SUTRA
- FEFLOW
- CODESA3D
- FEMWASTE
- FEMWATER

#### **2.7.2.1 SUTRA**

SUTRA is a finite-element computer code that was designed to simulate fluid movement and the transport of either energy or dissolved substances. The original version of SUTRA was released by Voss in 1984. SUTRA is based on a general physical, mathematical and numerical structure implemented using a computer code. Consequently, any modifications or additions can be done easily in this code such as; non-equilibrium sorption, chemical reactions, kinetic chemical reactions, etc. The SUTRA code was tested by simulating two benchmark problems: The Henry problem and the Elder problem, (USGS, 2010).

#### **2.7.2.2 FEFLOW**

FEFLOW is finite element software used to simulate 2-D and 3-D density depended flow, for mass and heat transport problems in groundwater. The first version of FEFLOW was released in 1979 and then became one of the most successfully known software in the field of hydrogeology. FEFLOW can simulate saturated, variably saturated, variable density and non-isothermal conditions, involving an arbitrary number of contaminants. FEFLOW simulates any solute transport problems based on advection and dispersion techniques and consider that any reaction is a kinetic reaction. FEFLOW has an advanced tool that does the solute transport problems called FEMATHED, (DHI-WASY, 2010).

#### **2.7.2.3 CODESA3D**

CODESA3D is a three dimensional finite element model that simulates flow and solute transport for variable density and variably saturated porous media domain. CODESA-3D is a combination between two computer codes; SATC3D (Saturated Coupled Flow and transport 3-Dimensional model) and FLOW3D (variably saturated Flow 3-Dimensional model). CODESA-3D simulates both flow and transport problems as coupled problems. The flow part calculates the water movement in the soil, taking into account different types of forcing inputs such as; infiltration/evaporation, recharge/discharge, withdrawal and injection, etc. While the transport part computes the migration of the solute plume due to advection, dispersion and diffusion processes, (Zheng and Bennett, 2002).

#### **2.7.2.4 FEMWASTE**

FEMWASTE is a two-dimensional finite element code that uses quadrilateral elements, to solve transport problems. FEMWASTE is designed to work with FEMWATER, (Zheng and Bennett, 2002).

#### **2.7.2.5 FEMWATER**

FEMWATER is a three-dimensional finite element code for density dependent flow and transport problems. It was produced by the authors of FEMWASTE, Yeh and Ward in 1980 (Zheng and Bennett, 2002).

#### **2.7.3 Code Selection**

Among the numerical codes reviewed here, SEAWAT was selected for the ease of operation that it offers. If we were modelling an existing aquifer with geometrically irregular boundaries, a finite-element code would be preferred, but since our aquifer is generic and of simple geometry by nature, a finite-difference code is favored as it will offer the same accuracy with the advantages of conceptual and numerical simplicity.

### **2.8 Summary**

From the previous discussion, the saltwater intrusion theory has been explained and the difference between sharp interface and a transition zone has been highlighted. According to Reilly and Goodman (1987), the type of transition zone depends on the ratio of freshwater lens thickness to total aquifer thickness. The theory of the up-coning phenomenon was investigated, and the difference between lateral intrusion and vertical up-coning was explained. From this literature review we found that most research was focused on finding analytical equations to describe the shape of the interface in static and transient conditions, however none of these methods are useful to investigate the actual impact of the saltwater presence on the response of freshwater. Numerical models were reviewed and SEAWAT was identified as the preferred tool for modelling both lateral intrusion and up-coning of saline intrusion for this project.



## **Chapter 3**

### **SEAWAT and Henry's Problem**

#### **3.1 Introduction**

SEAWAT is a two dimensional and three-dimensional finite-difference code, which was developed to simulate variable density, transient groundwater flow problems in porous media. The SEAWAT code is a combination of MODFLOW and MT3DMS gathered into a single program that solves the coupled flow and solute transport equations. In order to couple the groundwater flow equations with the solute transport equations SEAWAT uses either an explicit or an implicit technique.

SEAWAT was tested by simulating five bench mark problems; these include two box problems and three experimental problems namely; Henry's problem, Elder's problem and the HYDROCOIN problem. The SEAWAT results for the bench-mark problems were in good agreement with those obtained with the SUTRA finite element code, (USGS, 2002).

In this Chapter; a detailed discussion of the SEAWAT finite difference code is presented. The code development, governing equations, basic assumptions, discretization methods and benchmark problems will be explained. Henry's problem will be implemented and solved, and a comparison will be held between the solution to Henry's problem found in the SEAWAT user guide and our application to make sure that SEAWAT is being used properly.

### **3.2 Development of SEAWAT**

SEAWAT has been upgraded several times since it has been developed. The first version of SEAWAT was developed using MODFLOW-88, which was produced by McDonald and Harbaugh (1988) and MT3D, which was produced by Zheng in 1996. In the second version of SEAWAT a more recent version of MT3D called MT3DMS was used. MT3DMS was produced by Zheng and Wang in 1998. The second version also includes some improvements in the flow equation representation and in the boundary representation (Langevin and Guo, 1999). This second version was documented by Guo and Langevin in 2002 and was published by the U.S. Geological Survey (USGS). The third and last version of SEAWAT is SEAWAT2000, which was developed by combining MODFLOW-2000 and MT3DMS 1999. This latest version, also named SEAWAT4, included some new advancements and simulation options regarding how flow and solute transport are coupled. For example, in the previous version of SEAWAT the flow equation is solved at each transport time step regardless of whether there is a large change in fluid density or not. Now in SEAWAT V.4 there is an option that allows users to control how often the flow field is updated. Additionally, a new option has been implemented allowing the definition of a constant head boundary with the time variant Constant Head Package (CHD), which gives the option to express the boundary head as a function of the reference density associated with the concentration at the boundary. For example; if the user enters real heads, SEAWAT converts these head values to an equivalent freshwater head using the equilibrium relationship between freshwater and saltwater heads. If the solute concentration in the CHD defined boundary cell changes during the simulation the user has the option to fix the actual sea boundary head rather than the

equivalent freshwater head. This option increases the flexibility by allowing more control of boundary heads.

### **3.3 SEAWAT Mathematical Description and Development of Governing Equations**

The theory of variable-density groundwater flow is usually presented in terms of fluid pressure and fluid density. In SEAWAT, however, the groundwater flow equation is presented in terms of equivalent freshwater head and fluid density.

#### **3.3.1 SEAWAT Basic Assumptions**

Some basic assumptions were taken into account when developing the SEAWAT governing equations. These assumptions are as follow;

- a) Darcy's law is valid.
- b) The diffusion approach to dispersive transport is based on Fick's law.
- c) The flow and transport are under isothermal conditions.
- d) The porous medium is fully saturated with water.
- e) A single liquid phase of very small compressibility is assumed.

#### **3.3.2 Equivalent Freshwater Head Equations**

To develop the equivalent freshwater head equation we consider, two piezometers (A and B) that are opened at a virtual point N within a saline aquifer. Piezometer A contains fresh water and is supported with a mechanism that prevents saline water in the aquifer from mixing with the freshwater. Piezometer B contains water identical to that present in the saline aquifer. Figure 3-1 illustrates the equivalent freshwater head theory.

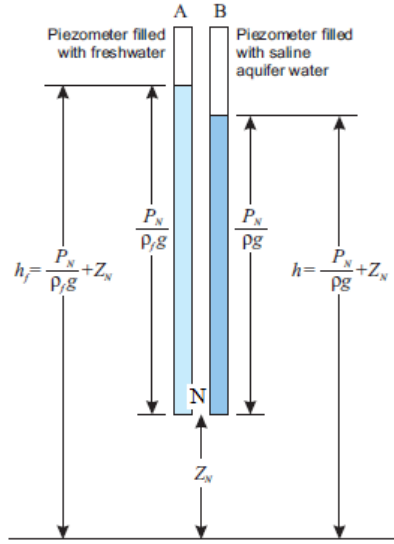


**Figure 3-1 Equivalent freshwater head (SEAWAT Guide, 2002)**

A datum is set and Bernoulli's equation is applied. The total freshwater head at piezometer A is calculated and the total saltwater head at piezometer B is determined at point N. Equations 3 and 4 represents the total head for piezometers A and B, respectively.

$$h_f = \frac{P_N}{\rho_f g} + Z_N \quad (3)$$

$$h_s = \frac{P_N}{\rho_s g} + Z_N \quad (4)$$

where;  $h_f$  is the freshwater head,  $h_s$  is the saltwater head,  $P_N$  is the pressure at point N and  $Z_N$  is the elevation head at point N.

By equating the pressure terms we get:

$$h_f = \frac{\rho_s}{\rho_f} h_s - \frac{\rho_s - \rho_f}{\rho_f} Z_N \quad (5)$$

$$h_s = \frac{\rho_f}{\rho_s} h_f + \frac{\rho_s - \rho_f}{\rho_s} Z_N \quad (6)$$

In SEAWAT the head values in a variable-density simulation are the equivalent freshwater head values.

### **3.3.3 Relationship Between $\rho$ and $C$**

Since SEAWAT is a combination of MODFLOW and MT3DMS, two basic governing equations are used,

- 1) General Flow Equation.
- 2) Solute Transport Equation,

In SEAWAT the aim of the coupling of these equations is to solve the variable density groundwater flow problems. This coupling process is based on creating a relationship between the solute concentration and the fluid density. This relationship is described by equations 9 and 10 below.

## **3.4 SEAWAT Governing Equations**

The General Flow Equation is derived by using the mass conservation law which states that the net rate of fluid mass flux into any control volume (REV) must be equal to the time rate of change of fluid mass storage within this element. Figure 3-2 and equations 7 to 14 explain the coupling procedure applied in SEAWAT .

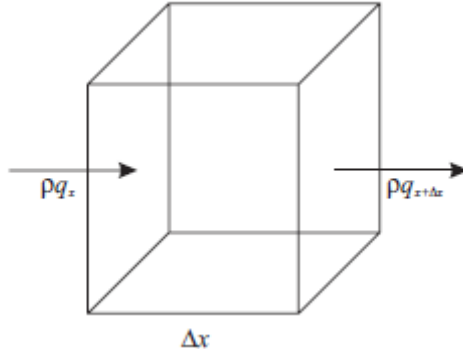


**Figure 3-2 Representative Elementry Volume in porous medium (SEAWAT Guide, 2002)**

$$-\frac{\partial \rho q_x}{\partial x} - \frac{\partial \rho q_y}{\partial y} - \frac{\partial \rho q_z}{\partial z} = \partial \frac{\rho \theta}{\partial t} \quad (7)$$

By using differentiation by parts for the right hand side of the previous equation

$$\therefore -\frac{\partial \rho q_x}{\partial x} - \frac{\partial \rho q_y}{\partial y} - \frac{\partial \rho q_z}{\partial z} = \theta \frac{\partial \rho}{\partial t} + \rho \frac{\partial \theta}{\partial t} \quad (8)$$

$$\cdots \rho = f(P, C) \quad \rho = \rho_f + EC \quad (9)$$

$$E = \frac{\partial \rho}{\partial C} = 0.7143 \quad (10)$$

$$\frac{\partial \theta}{\partial t} = \frac{\partial \theta}{\partial P} \times \frac{\partial P}{\partial t} \quad (11)$$

$$\frac{\partial \rho}{\partial t} = \frac{\partial \rho}{\partial P} \times \frac{\partial P}{\partial t} + \frac{\partial \rho}{\partial C} \times \frac{\partial C}{\partial t} \quad (12)$$

$$\partial \frac{\rho \theta}{\partial t} = \rho S_s \frac{\partial P}{\partial t} + \theta \frac{\partial \rho}{\partial C} \times \frac{\partial C}{\partial t} \quad (13)$$

$$\therefore -\frac{\partial \rho q_x}{\partial x} - \frac{\partial \rho q_y}{\partial y} - \frac{\partial \rho q_z}{\partial z} = \rho S_s \frac{\partial P}{\partial t} + \theta \frac{\partial \rho}{\partial C} \times \frac{\partial C}{\partial t} \quad (14)$$

Starting from equation (13) the right hand side is now a function of fluid density and solute concentration. The left hand side also can be written as a function equivalent freshwater heads using Darcy's Law. Equations 15,16, and 17 explain the steps that lead to the general equation that is used in the SEAWAT code .

$$q_x = -KiA \quad (15)$$

$$K_{ij} = \frac{k\rho g}{\mu} \quad (16)$$

$$\therefore q_x = -K_x \frac{\mu_f}{\mu} \left[ \frac{\partial h_f}{\partial x} \right] \quad (17)$$

SEAWAT has an option to redirect the hydraulic conductivity axes to the general global axes automatically, by adjusting the  $K$  angles from  $\alpha, \beta, \gamma$  (aquifer axes) into general global axes ( $X, Y, Z$ ). Equation 18 represents the final general flow equation for SEAWAT in any direction with any aquifer inclination angles in terms of freshwater head, fluid density and solute concentration.

$$\begin{aligned} & \frac{\partial}{\partial x} \left( \rho K_{f\alpha} \left[ \frac{\partial h_f}{\partial \alpha} + \frac{\rho - \rho_f}{\rho_f} \cdot \frac{\partial z}{\partial \alpha} \right] \right) + \frac{\partial}{\partial \beta} \left( \rho K_{f\beta} \left[ \frac{\partial h_f}{\partial \beta} + \frac{\rho - \rho_f}{\rho_f} \cdot \frac{\partial z}{\partial \beta} \right] \right) \\ & + \frac{\partial}{\partial \gamma} \left( \rho K_{f\gamma} \left[ \frac{\partial h_f}{\partial \gamma} + \frac{\rho - \rho_f}{\rho_f} \cdot \frac{\partial z}{\partial \gamma} \right] \right) \\ & = \rho S_s \frac{\partial h_f}{\partial t} + \theta \frac{\partial \rho}{\partial C} \cdot \frac{\partial C}{\partial t} - \bar{\rho} q_s \end{aligned} \quad (18)$$

Since the groundwater flow causes a redistribution of the solute concentration, which alters fluid density, both the general flow equation and solute transport equations must be solved simultaneously. The solute mass is transported in porous media by the flow of groundwater (advection), mixed by the molecular diffusion process and spread by the mechanical

dispersion. The three processes occur simultaneously, and are described by the transport equation (19).

$$\frac{\partial c}{\partial t} + \frac{\partial C}{\partial x_i} v_i - \frac{\partial}{\partial x_i} \left( D_{ij} \frac{\partial C}{\partial x_{ij}} \right) = \pm \frac{G}{\theta} \quad (19)$$

### 3.5 SEAWAT Discretization Methods

#### 3.5.1 Spatial Discretization Scheme

The SEAWAT code has two types of discretization schemes. A spatial discretization scheme and a temporal discretization scheme. In spatial discretization, the flow processes and the transport process require specific information about the finite difference grid such as column width, cell height and layer thickness. The grid information must be specified as an input into two separate files if the MT3DMS transport is used before running SEAWAT. Because the latest version of SEAWAT (SEAWAT-2000) cannot verify if the grid information is consistent in both MODFLOW and MT3DMS transport process, Pre- and -post-processor programs such as Groundwater Vistas were used for this project do this automatically. The users should make sure that the spatial discretization information is consistent.

#### 3.5.2 Temporal Discretization Scheme

The temporal discretization scheme used by SEAWAT is a combination between two temporal discretization schemes, a temporal scheme used in conventional MODFLOW and a MT3DMS temporal scheme. In the conventional MODFLOW code; the total simulation



period is divided into one or more stress periods. During the simulation for each single stress period, input flow rate and the boundary conditions remain constant unless a time-varying B.C is defined through the CHD package. In each stress period the time is divided into one or more timestep size to produce results that are more accurate or allow model output to be saved for the selected time. During each timestep, MODFLOW solves the flow equation for the period from  $t_n$  to  $t_{n+1}$ , using an implicit formulation.

MT3DMS further divides the MODFLOW time step into transport steps. The term transport step is used to avoid confusion with a MODFLOW timestep. The transport step is a time increment that is used by MT3DMS to solve the solute transport equation. The transport step length in MT3DMS are not specified by the user. They are calculated by the program to ensure stability especially when calculating the advection flux. For a given MODFLOW timestep extending from  $t_n$  to  $t_{n+1}$ , MT3DMS uses the values of velocity calculated for the end of the timestep  $t_{n+1}$  to calculate the length and number of transport step required over the interval  $t_n$  to  $t_{n+1}$ . The time steps are calculated to ensure that the Courant number is proportional to the grid size. In SEAWAT, the Courant Number is the ratio of the advective distance during one time step to the spatial discretization distance and must be smaller than or equal to one.

### **3.6 Flow and Transport Coupling**

In the previous section, the timestepping approach that is used in MODFLOW and MT3DMS is discussed. This section provides an explanation of the coupling process between MODFLOW and MT3DMS in SEAWAT. The coupling process between the flow and transport equations can be achieved in SEAWAT by either of the following two approaches.

- a) Explicit Coupling.

b) Implicit Coupling.

### 3.6.1 Explicit Coupling of Flow and Transport

In the explicit coupling approach, the flow equation is solved iteratively using modified MODFLOW routines to calculate heads at time  $t_1$  as an initial timestep. This iterative solution procedure is performed with the fluid densities from the previous stress period. If this is the first time step, then the densities calculated from the initial concentration  $\rho_0 = f(C_0)$  are used. The length of the initial time step,  $\Delta t_1$  is specified by the users either by the INTIALDPT option or by the code default option. The code default value is 0.01 and the time unit specified by users are seconds, minutes, hours, days or years. The specific discharge values for time  $t_1$  at the model boundaries and within the model domain are calculated from the results of the flow simulation and passed to the transport routines to represent the flow over the time interval  $\Delta t_1$ . The solute concentration for the time  $t_1$  is solved over the time interval  $\Delta t_1$ . The fluid densities used in solving the flow equation for the second timestep are calculated from  $t_1$  solute concentration. The length of  $\Delta t_2$  is calculated based on the stability and accuracy requirements by using the values of velocities that had been calculated from for the beginning of that time period. The length of  $\Delta t_2$  should always be greater than  $\Delta t_1$  and if it is less, SEAWAT will display a warning message. The heads and flows that are being solved by the flow equation at timestep  $t_2$  are based on the fluid densities that have been calculated in the first timestep. The solute concentrations for time  $t_2$  are determined by solving the transport equation over the time interval  $\Delta t_2$  and the fluid densities that are used are calculated from time  $t_2$ . The sequence is repeated for  $\Delta t_3$  and until the simulation process is completed. Figure 3-3 illustrates the explicit scheme in SEAWAT (USGS, 2000).

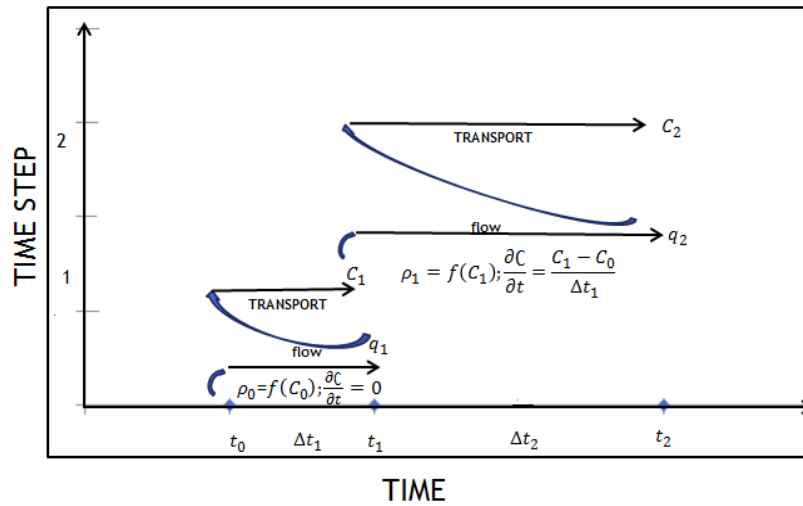


**Figure 3-3 Explicit scheme for coupling in SEAWAT (SEAWAT Guide, 2002)**

Although the explicit coupling approach requires less computer time, instability problems may occur during the solution of the flow equation, as the calculated densities use the concentrations from the previous timestep. Also the lengths of timesteps, which are calculated to satisfy the stability constraints and accuracy requirements of the transport equation, are based on velocities calculated for the end of the preceding timestep.

### 3.6.2 Implicit Coupling of Flow and Transport

In the implicit coupling approach the flow equation and the transport equation are solved iteratively for each time step, until the consecutive difference in the calculated fluid densities are less than user specified values. Figure 3-4 shows the implicit coupling approach scheme in SEAWAT.

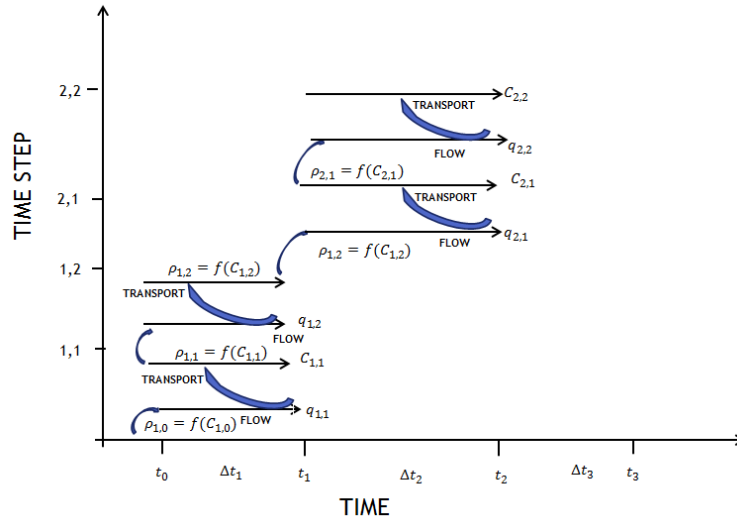


**Figure 3-4 Implicit coupling approach scheme (SEAWAT Guide, 2002)**

Like with the explicit approach, the values of specific discharge for time  $t_1$  at the model boundaries and within the model domain are calculated from the results of the flow simulation and passed to the transport routines to represent the flow over the time interval  $\Delta t_1$ . Solute concentrations for time  $t_1$  are determined by solving the transport equation over the time interval  $\Delta t_1$ . The fluid densities for  $t_1$ , which are used in solving the flow equation for the second time step, are calculated from the  $t_1$  solute concentrations. In the implicit coupling approach the heads, concentrations, densities and flow results pertain to the end of the time step. In the current version of SEAWAT, the implicit coupling approach can't be used if the simulation includes particle tracking or particle-based solution methods. If the implicit approach was used in a particle based solution, an advanced computer memory would be required to store particle information, once the implicit coupling approach may solve the transport equation more than one time for each time step. In the implicit coupling approach the user may specify the lengths of the coupling time steps.

The Implicit coupling approach has a matrix solver called Generalized Conjugate Gradient (GCG). This GCG solver is used in conventional MT3DMS to increase the length of transport steps, reduce the number of the transport steps and substantially reduce the amount of time required for a computer to perform the simulation.

### **3.7 SEAWAT Benchmark Problems**

SEAWAT was verified by running five different problems and the results have been compared with other variable- density codes. The SEAWAT verification problems have been classified into two categories, Box problems and Benchmark problems. These problems are listed as follow;

- a) Two Cases of Box Problems (Voss and Souza, 1987).
- b) Elder's Problem (Voss and Souza, 1987).
- c) HYDROCOIN Problem (Konikow *et.al.*, 1997).
- d) Henry's Problem (Voss and Souza, 1987).

#### **3.7.1 Box Problems**

The main purpose of simulating the SEAWAT box problems using SEAWAT is to ensure that fluid densities are properly calculated. The box problems also measure how good the approximation of the finite difference grid is. There are two different cases of the box problems. The first case simulates flow within a two- dimensional vertical cross section with no-flow boundaries on both sides. The hydraulic conductivity and the porosity values are not important and the diffusion coefficient and the transverse dispersivity are set to zero. In the second case, the horizontal flow that is induced by specifying different types of hydrostatic constant heads on the left and right sides of the box is calculated.

### **3.7.2 Elder's Problem**

Elder's problem was mainly designed for heat flow by Elder (1967); however Voss and Souza adjusted the problem in 1987 to be valid for variable-density groundwater codes. Elder's problem has been solved by SEAWAT and SUTRA and both codes result in a good match to each other (Simpson and Celement, 2002).

### **3.7.3 HYDROCOIN Problem**

Konikow and others developed a project called Hydrologic Code Intercomparison or (HYDROCOIN) to evaluate the accuracy of the selected groundwater codes. The problem that was represented in SEAWAT is based on case 5 of the HYDROCOIN project, which was re-evaluated with the MOC DENSE code. The results by the SEAWAT code were in a good agreement with the MOC DENSE code results, (USGS, 2002).

### **3.7.4 Henry's Problem**

In 1964 Henry presented an analytical solution for groundwater flow in a coastal aquifer. Henry's problem has been simulated numerically as a reference problem by many numerical codes. In 1993 Segol showed that Henry's analytical solution was not exact as he eliminated mathematical terms from the solution, believed to be insignificant. Segol showed that numerical codes such as SUTRA can provide a more accurate solution for Henry's problem. Henry's problem has been taken as a first step in our simulation to verify that SEAWAT has been used properly and our results have been compared with those presented in the SEAWAT manual results, (USGS, 2002).

### 3.8 Testing Against Henry's Problem

#### 3.8.1 Model Formulation and Description

The domain is a 2-m long cross sectional box by 1-m high and by 2-m wide. A constant flux of freshwater is applied to the left boundary at a rate of 5.702 m<sup>3</sup>/d per meter with zero C<sub>in</sub> concentration. At the right side of the box a constant head boundary represents seawater hydrostatic conditions. The upper and lower model boundaries are no flow. Figure 3-5 illustrates the Henry's problem model parameters and conditions.

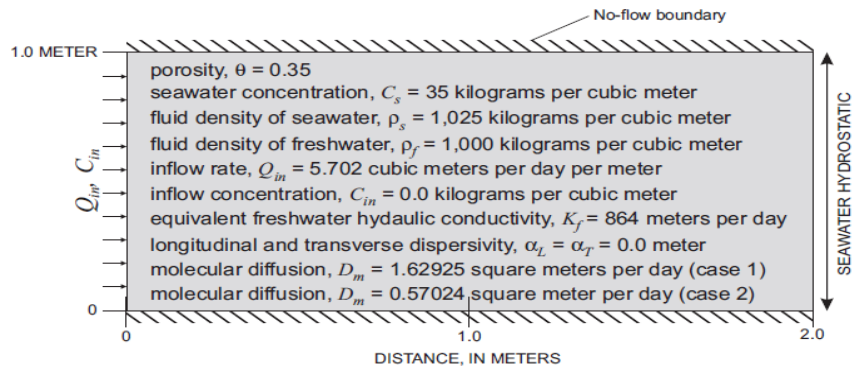
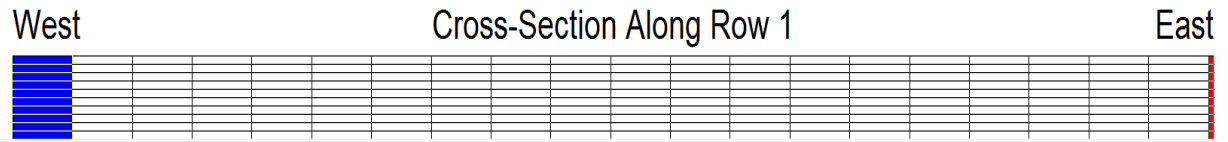


Figure 3-5 Henry's problem model parameters (SEAWAT Guide, 2002)

#### 3.8.2 Finite Difference Grid Description

In Henry's problem the solution domain consists of one row divided into ten layers and 21 columns. Each cell with the exception of cells in column 21 are 0.1 by 0.1 m in size, the cells in columns 21 are 0.01-m horizontal by 0.1-m vertical. The narrow cells in column 21 were used to represent the seawater hydrostatic boundary at the end of the 2-m box. Figure 3-6 shows an elevation view for the Henry's problem run by SEAWAT, (SEAWAT Guide, 2002).



**Figure 3-6 Henry's problem finite-difference grid**

### **3.8.3 Boundary Conditions and Model Implementation**

The Henry problem caused much discussion and confusion among the modelling community about the real value of molecular diffusion that had been used by Henry. In the Henry problem two cases were modeled. In the first case the molecular diffusion was given a value of  $D_m = 1.62925 \text{ m}^2/\text{d}$ , while in the second case the  $D_m$  value =  $0.57024 \text{ m}^2/\text{d}$ . Only the first case was considered in the current study. Two types of boundary conditions have been used. For the freshwater side a well boundary (specified flux) condition has been used with a flow rate for each layer equal to  $0.057024 \text{ cm}^2/\text{d}$ , while, for the saltwater side a constant head of 1m with constant concentration of ( $35 \text{ kg/m}^3$ ) were specified. The initial concentration has been set at  $35 \text{ kg/m}^3$  everywhere. An implicit coupling approach has been used with total time to reach steady state of 0.24 d. The total flow time step number is 3000 with a time step multiplier of 8. For MT3DMS a (TVD) approach has been used for the advection term. The Courant number  $c_r$  was set to 0.1 which equals the grid spacing between the cells, to achieve more balance in the simulation of solute transport across the cells. Figure 3-7 illustrates the elevation view for the concentration distribution in the Henry problem run by SEAWAT. Table 3-1 summarizes the Henry problem flow and numerical parameters, (Langevin and Guo, 2006).



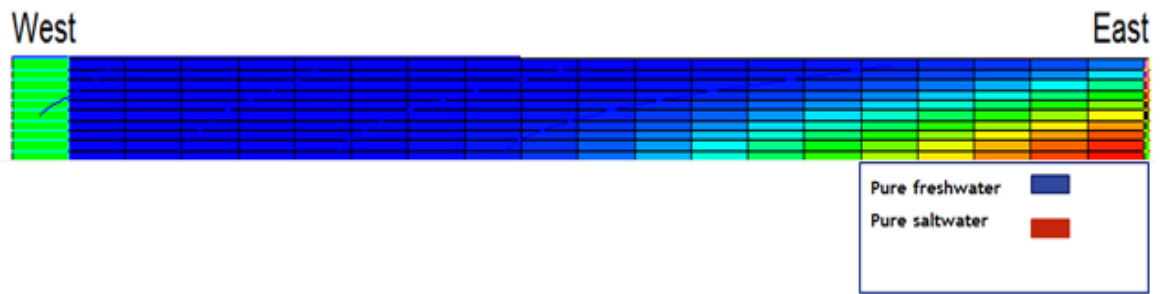


**Figure 3-7 Henry's problem concentration distributions**

**Table 3-1 Input and Numerical solution parameters for the Henry's problem, (Langevin and Guo , 2006)**

<b>Parameter</b>	<b>Value</b>
<b>Flow Parameters</b>	
$Q_{in}$	5.702m <sup>2</sup> /d
$C_{in}$	0.0 Kg/m <sup>3</sup>
$K_f$	864m/d
$n$	0.35
$\alpha_t$ & $\alpha_l$	0m
$D_m$	1.62925m <sup>2</sup> /d
$C_s$	35Kg/m <sup>3</sup>
$\rho_s$	1025Kg/m <sup>3</sup>
$\rho_f$	1000Kg/m <sup>3</sup>
<b>Numerical solution parameters</b>	
Cell size(coulmn1to20);dx,dz	0.1X 0.1m
Cell size (coulmn21);dx,dz	.01 X 0.1m
<b>Solution of flow equation</b>	
Matrix solution technique	PCG
Head convergence value	1 X 10 <sup>-7</sup> m
Flow convergence value	1 X 10 <sup>-7</sup> kg/d
<b>Solution of transport equation</b>	
Advection term	TVD
Dispersion and source terms	Implicit finite difference ; GCG
Time-step length	Caluclated during simulation using Cr=0.1
Concentration convergence value	1 X 10 <sup>-6</sup>

### 3.8.4 Results and Comparison

Although a perfect match was not achieved due to the difference in time step size between the original Henry problem and the applied ones, the results provide a validation to confirm the performance of our implementation of SEAWAT. Figure 3-8 shows the comparison between the applied Henry problem and the original one published in the SEAWAT user manual.

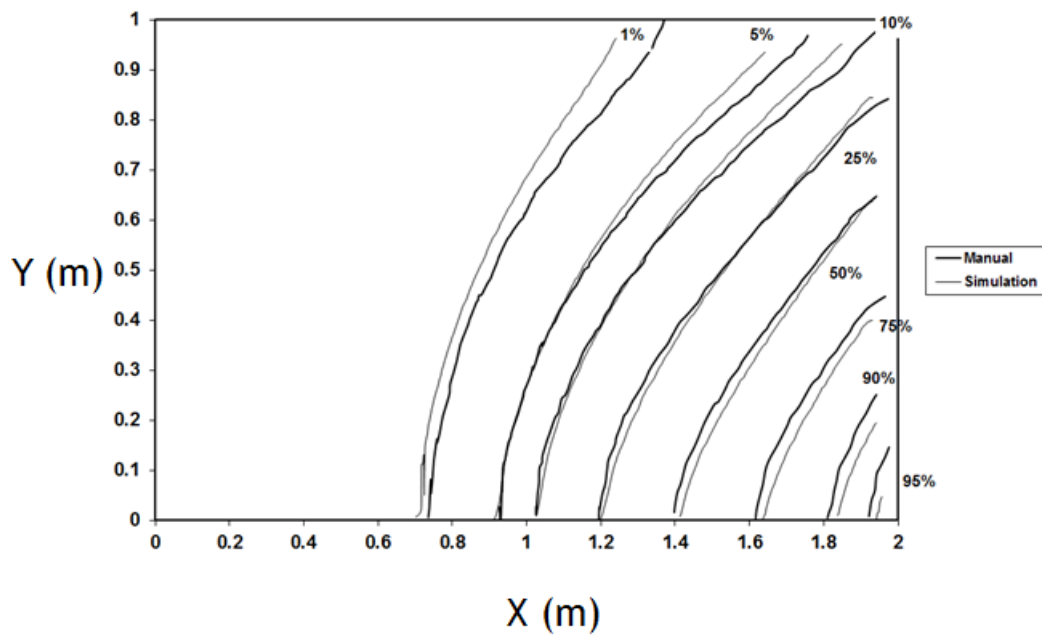


**Figure 3-8 Comparison between published Henry's problem solution and SEAWAT solution to the Henry's problem**

## Chapter 4

### Coastal Aquifer Model Description and Verification

#### 4.1 General Purpose and Scope

Most coastal zones around the world are subjected to irregular precipitation throughout the year. Modeling a coastal aquifer under different precipitation rates is a complicated problem as the thickness of the freshwater lens is influenced by precipitation and pumping. The shape and the position of the interface between salt and freshwater have been studied both analytically and numerically. The Ghyben – Herzberg (G&H) relationship, explained in detail in chapter two, was the first theory to establish a ratio of 1:40 for the fresh and saltwater upper boundary elevations based on their density differences. The G&H relationship can be applied for steady state and transient conditions with and without pumping. During pumping, an up-coning is formed underneath the pumping well and the ratio between the drop in freshwater and the saltwater rise is governed by the G&H relationship.

In this chapter, a two dimensional homogeneous and isotropic model is developed to represent a generic saltwater island aquifer using SEAWAT. The model results are compared to the G&H relationship in order to validate the model in steady state and transient conditions. The model results show an excellent agreement with the G&H theoretical values. This validation provides support for future simulation scenarios.

## 4.2 Saltwater Model Formulation and Description

### 4.2.1 Model Area and Mesh Description

The two dimensional model is 2.5 km-long, 150 m thickness and 25 m wide. The aquifer model consists of 15 layers of 10m thickness each. The 2D model has 100 columns and one row. The model top elevation is 9 m and the bottom elevation is -141 m. The negative sign indicates an elevation below sea level. The cell size is 25 by 25 m by 10 m thick, the grid is uniform. Figure 4-1 illustrates the 2D saltwater model dimensions.

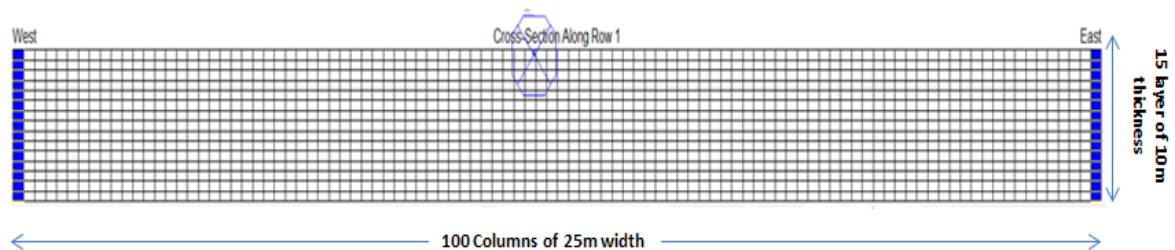


**Figure 4-1 Model dimensions**

### 4.2.2 Model Hydrological Parameters

The generic saltwater model is an unconfined coarse sand homogenous and isotropic aquifer; the model hydraulic conductivity was set at 45 m/day. The soil effective porosity is 0.28, the specific storage is 0.001, and the aquifer specific yield is 0.2. The aquifer longitudinal dispersivity is 2.5 m and the transverse dispersivity is 0.25 m. The initial salt concentration for the model is homogenous and is equal to 35 kg/m<sup>3</sup>. The distribution factor  $K_d$  for the original saltwater chemical composition is 0.0086. Because we wanted a sharper interface model, the diffusion coefficient was set to a small value of 0.001m<sup>2</sup>/day.

### **4.2.3 Model Boundary Conditions**

A uniform recharge is applied over the aquifer surface area with a rate 0.005 m/day. The unconfined aquifer consists of 15 layers. A zero meter constant head boundary condition has been applied along both lateral boundaries. The concentration at the boundary was constant and equal to 35 kg/m<sup>3</sup>. A no-flow boundary condition is set by default at the bottom of the aquifer. A monitoring well has been set almost in the middle of the aquifer, at a distance X=1200 m. The well is set in the first layer to measure the fluctuations in the freshwater head. The simulation was transient with a total time around 124 years divided into five stress periods. The first stress period was 123 years, which was long enough to achieve stable conditions to develop a steady-state freshwater lens. Then four stress periods of 100 day each have been set up to test the response of the aquifer to pumping.

### **4.2.4 Model Numerical Flow and Transport Solution Approach**

The simulation was performed with SEAWAT. An implicit coupling approach has been used and a finite difference solution scheme has been applied for the transport component. The implicit approach was selected to avoid the instability problems that may occur during solution of the flow equation.

The maximum value of (1) for the Courant number has been used. The temperature effect was neglected so the VSC option has not been used. For the VDF package a “1-species -1 coupled flow and transport” has been used as only 1 solute (Sodium-chloride) is present. The reference fluid density (DENSESLP) was set to 1000. Figure 4-2 illustrates the 2D saltwater/freshwater generic aquifer at steady state and table 4-1 summarizes saltwater model flow and numerical parameters.

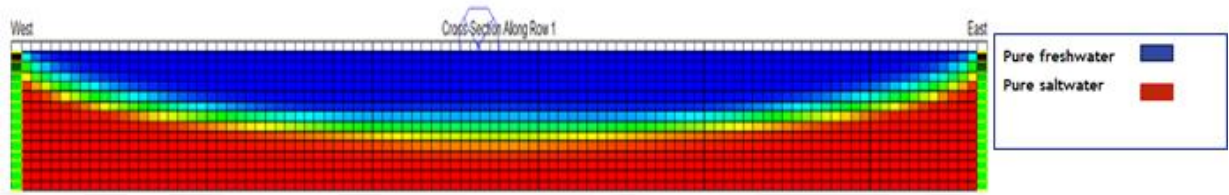


**Figure 4-2 2D saltwater/freshwater generic aquifer model**

**Table 4-1 Input and Numerical solution parameters for the saltwater generic aquifer model**

Parameter	Value
<b>Flow Parameters</b>	
$K_x=K_y=K_z$	45m/day
$n$ effective porosity	0.28
$S_s$	0.001
$S_y$	0.2
$\alpha_l$	2.5 m
$\alpha_t$	0.25 m
D	0.001 m <sup>2</sup> /day
$C_{ini}$	35 kg/m <sup>3</sup>
$K_d$	0.0086
R	0.005 m/day
$\rho_s$	1025 Kg/m <sup>3</sup>
$\rho_f$	1000 Kg/m <sup>3</sup>
<b>Numerical solution parameters</b>	
Cell size(coulmn1to100);dx,dy	25 X25m
Well distance from west of boundary	1200m
<b>Solution of flow equation</b>	
Matrix solution technique	PCG
Head convergence value	1 X 10 <sup>-7</sup> m
Flow convergence value	1 X 10 <sup>-7</sup> kg/d
<b>Solution of transport equation</b>	
Advection term	Finite difference
Dispersion and source terms	Implicit finite difference ; GCG
Time-step length	10days
Courant number	Cr=1
Concentration convergence value	1 X 10 <sup>-6</sup> Kg/m <sup>3</sup>

### 4.3 Model Verification

The G&H relationship was used to verify the validity of the current model before it was used in the research scenarios. The model was tested against the G&H relationship in both steady state and transient conditions. As a sharp interface is impossible to develop in reality and



numerically, the location of the interface during our simulations was taken as the position of the contour of 50% concentration (Tain et. al., 1997).

### 4.3.1 Steady State Verification

Heads and concentration profiles have been taken along columns 46 and 85 when there is no pumping and after the first stress period has ended. The monitored columns were selected to cover the most critical locations/cells in the model to give a clear view of the head fluctuation along these sections. For example, Column 46 is at the middle of the model and the furthest away from the lateral boundaries. Column 85 is located closer to the right boundary and will provide a test of our model behaviour closer to a boundary. Figure 4-3 illustrates the positions of the monitored columns.

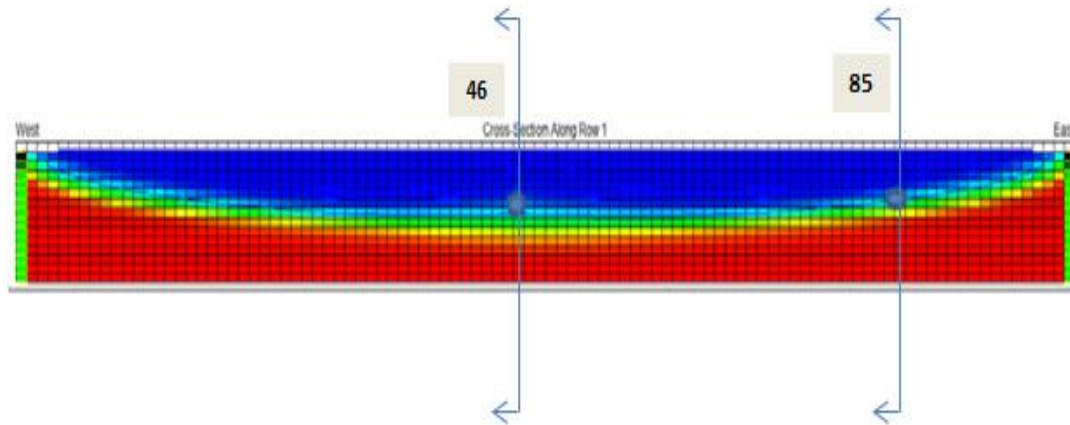


**Figure 4-3 Illustration the selected columns**

In order to obtain the elevation where the concentration is at 50% within each monitored column, a linear interpolation was done with Excel.

For column 46; the steady-state water table elevation was 1.8 m. while the elevation of the interface (50% concentration) was at -72.4 m, which is 1% off the elevation of -72 m predicted by the G&H relationship.

The same calculations were completed for column 85; the water table rose to 1.43m while the interface was at an elevation of -56.8, which is again roughly 1% off the G&H-predicted value of -57.2 m.

### 4.3.2 Transient Verification

The model was tested for transient conditions to observe the up-coning that occurred due to pumping. A pumping well was placed in column 46 and the well screen (location of water withdrawal) was placed in layer 1. Elevations before and after pumping were observed and the G&H relationship was verified.

Without pumping and with a recharge rate of 0.005 m/day the freshwater head elevation starts at 1.8 m and the saline interface (50% concentration) is at -72.4 m. With pumping applied at 100 m<sup>3</sup>/day for 100 days, the freshwater head elevation became 0.65 m and the elevation at 50% concentration was at -26.37 m. Equations 20 to 23 and figure 4-4 illustrate the G&H relationship when the up-coning occurred.

The change in freshwater head due to pumping  $\Delta h_f$ ,

$$\Delta h_f = 1.8 - 0.65 \cong 1.15 \text{ m} \quad (20)$$

The observed up-coning is  $\Delta z_s$ ,

$$\Delta z_s = 72.4 - 26.3 \cong 46.1 \text{ m} \quad (21)$$

From the Ghyben – Herzberg relationship;

$$\Delta z_s = 40 \Delta h_f \quad (22)$$

Using the observed elevations,

$$\Delta z_s = 40 * 1.15 = 46 \text{ m} \quad (23)$$

The predicted  $\Delta z_s$  is within 1% of the observed  $\Delta z_s$ , further validating the model.

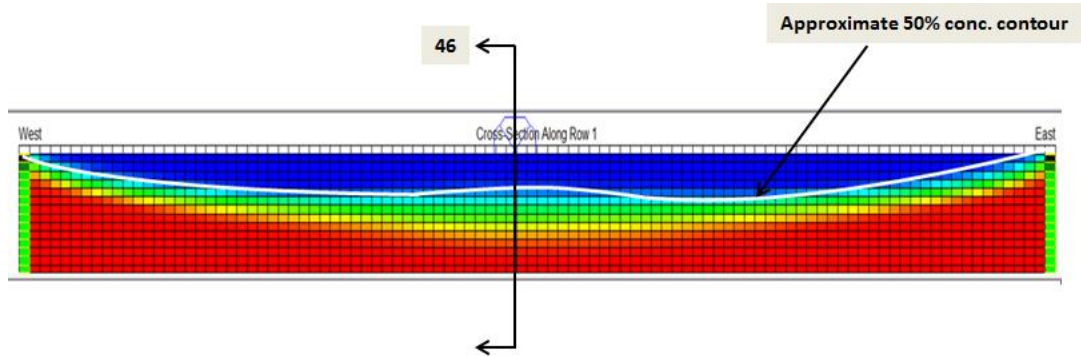


**Figure 4-4 Model output showing up-coning during pumping**

#### **4.4 Summary**

From the simulations presented above, the developed model results were verified against the G&H relationship and were shown to be in agreement in both steady state and transient conditions. The model is now reliable and can be used for further simulations.

## **Chapter 5**

### **Development and Verification of Equivalent Freshwater Models**

#### **5.1 Introduction**

In a previous chapter, the 2D model was developed and tested against the G&H relationship and the model results were in a good agreement with the G&H theoretical values. In the next phase of work, the model was used to investigate the effect of the saltwater presence on the behavior of the aquifer. The general approach was to develop a two dimensional freshwater model similar to the saltwater/freshwater version discussed in the previous chapter, and to compare the behavior of the freshwater components of each model to identify possible relationships that would support the development of an equivalent modeling approach. The models were tested for different sand types and under different pumping and recharge rates. Table 5-1 presents the hydraulic conductivity values according to sand type. A general trend was obtained between the real and the equivalent freshwater hydraulic conductivities for different sand types.

Subsequently, a three dimensional homogeneous and isotropic model was developed, to test the validity of the equivalent freshwater hydraulic conductivities under different pumping scenarios.

**Table 5-1 Representative hydraulic conductivity values for different sand soil types (Morris and Johnson, 1967)**

<b>Soil type</b>	<b>Hydraulic conductivity K (m/day)</b>
Fine sand	2.5
Medium sand	15
Coarse sand	45

The freshwater/saltwater model was simulated using SEAWAT while the pure freshwater model was simulated with MODFLOW only.

## **5.2 2D Freshwater Model Investigation**

The test case is a two dimensional homogeneous and isotropic model simulated by using MODFLOW. No coupled solute transport simulation is performed. The freshwater model is similar to the saltwater model described in the previous chapter; however, it has different boundary conditions. The heads at the side boundary are different and depend on the layer elevation. Table 5-2 summarizes the freshwater model geometrical, flow and numerical parameters.

**Table 5-2 Input and Numerical solution parameters for the freshwater generic aquifer model**

Parameter	Value
<b>Flow Parameters</b>	
$K_x=K_y=K_z$	variable
$n$ effective porosity	0.28
$S_s$	0.001
$S_y$	0.2
R	0.005 m/day
$\rho_f$	1000 Kg/m <sup>3</sup>
<b>Numerical solution parameters</b>	
Cell size(column1to100);dx,dy	25 X25 m
Well distance	1200 m
<b>Solution of flow equation</b>	
Matrix solution technique	PCG
Head convergence value	1 X 10 <sup>-7</sup> m
Flow convergence value	1 X 10 <sup>-7</sup> kg/d

In order to impose boundary conditions that are equivalent to those of the saltwater model, the freshwater equivalent heads were computed and applied at each layer using equation (24), which is a reduced form of equation (6), presented in chapter 3. These head values were calculated based on the difference in density between saltwater and freshwater and the layer middle elevation. Figure 5-1 illustrates the equivalent freshwater model boundaries.

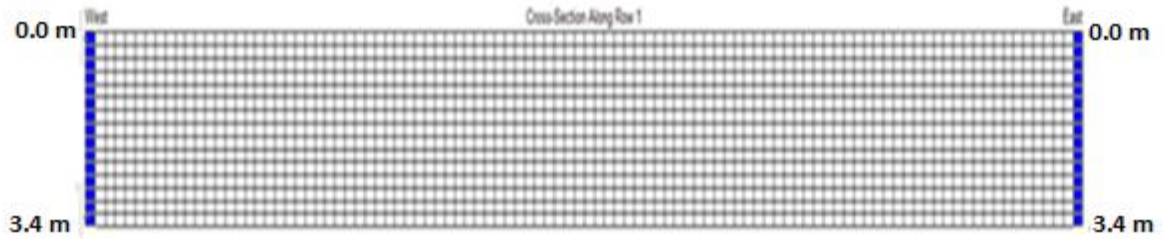


**Figure 5-1 Equivalent freshwater head distribution at constant –head boundaries  
for the freshwater generic model**

The equivalent fresh water head  $h_{ef}$  at the boundary was computed with:

$$h_{ef} = -0.025Z \quad (24)$$

Where;  $Z$  is the elevation at the middle of each layer.

The boundary head in the top layer was set at 0 m.

### 5.2.1 Methodology

This section summarizes the general steps that were applied, to study the effect of the saltwater presence on the aquifer behaviour to develop the relationship between the real hydraulic conductivity  $K_s$  and the equivalent freshwater hydraulic conductivity  $K_f$ . The general relationship between  $K_s$  and equivalent  $K_f$  was generated under two recharge rate values - ( $R$ ) - of 0.005 m/day and 0.008 m/day. Each recharge rate gives different freshwater lens thicknesses ( $B_f$ ). Each recharge rates represented a simulation set and in each set the simulations were performed with the freshwater/saltwater model for a range of Hydraulic Conductivities ( $5 \text{ m/day} \leq K_s \leq 45 \text{ m/day}$ ). Different values of pumping rates ( $Q$ ) were applied for each recharge sets and these represent scenarios ( $a$  to  $e$  and  $f$  to  $j$ ).

Freshwater-only model runs were then performed for each recharge sets and pumping scenarios. The hydraulic conductivity of these models was changed until a best match was

achieved between the saltwater/freshwater model and the freshwater-only model. This yielded the Equivalent Freshwater Hydraulic Conductivity  $K_f$  applicable to each scenario. Finally; the  $K_f$  values so obtained were plotted against the  $K_s$  values for all  $Q/B_f$  ratios and for each recharge conditions.

### 5.2.2 First Simulation Set

In the first scenario a 0.005 m/day recharge was imposed. The average corresponding steady state freshwater lens depth  $B_f$  calculated at 50% salt concentration, for the different sand types, was 50 m. Five different pumping Scenarios (*a, b, c, d and e*) were applied to the saltwater/freshwater model to generate five ratios for  $Q/B_f$ . Each pumping rate applied is used to test the effect of saltwater presence on the different sand types ( $K_s = 5, 10, 15, 20, 25, 30, 35, 40$  and  $45$  m/day). Table 5-3 summarizes the pumping amounts for different  $Q/B_f$  ratios for the salt/freshwater model.



**Table 5-3 Ratios of  $Q/B_f$  for first simulation set**

<i>Recharge Rate</i> $R = m/day$	<i>Pumping rates</i> $Q = m^3/day$	<i>Approximate pure Freshwater lens (<math>B_f</math>)</i>	<i>(<math>Q/B_f</math>) Ratio</i>
$R = 0.005 m/day$	a) 100	50 m	2
	b) 200		4
	c) 300		6
	d) 400		8
	e) 500		10

Pumping was initiated in the third stress period, to provide the model sufficient time for drawdown and recovery and to provide a clear indication of head fluctuations. Throughout the simulation the sand was divided into nine groups starting from fine sand ( $K_s = 5 m/day$ ) to very coarse sand ( $K_s=45 m/day$ ). The intent was to cover most sand types to obtain a reliable indication of saltwater behaviour for a wide range of aquifers. The following sections show only the determination of  $K_f$  for two pumping scenarios ( *a* & *b*) and two  $K_s$  values (5 and 10 m/day).

#### 5.2.2.1 Pumping Scenario (a)

For fine sand with  $K_s$  equal to 5 m/day, the corresponding equivalent  $K_f$  value based on the minimum RMSE, is 5.5 m/day. Table 5-4 illustrates the minimal RMSE determination among different  $K_f$  values and figure 5-2 shows a plot of the best fit between the two models. The head profiles used for comparison and RMSE computation were recorded at a monitoring well

located in the first layer at the middle of the aquifer. Equation (25) presents the root mean square error formula.

$$RMSE = \sqrt{\frac{\sum(h_f - h_s)^2}{N}} \quad (25)$$

where:

$h_s$  : Saltwater head

$h_f$ : Freshwater head

$N$ : Number of time steps in the simulation interval used to compute the RMSE

**Table 5- 4 Optimum  $K_f$  value determination for  $K_s= 5$  m/day**

$K_s$ (m/day)	$K_f$ (m/day)	RMSE
5	5.2	0.237
5	5.3	0.146
5	5.4	0.060
5	5.5	0.038
5	5.6	0.115

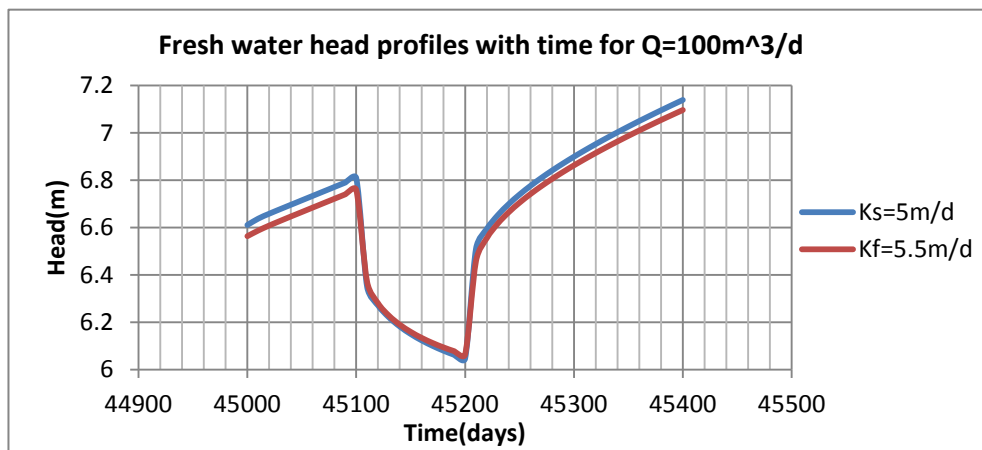


**Figure 5-2 Water table response comparison for (a) pumping scenario when  $K_s = 5$  m/day**

The same process was completed for  $K_s = 10$  m/day and the equivalent freshwater hydraulic conductivity was 11.8 m/day. Table 5-5 illustrates the minimal RMSE determination among different  $K_f$  values and figure 5-3 shows a plot of the best fit between the two models.

**Table 5-5 Optimum  $K_f$  value determination for  $K_s= 10$  m/day**

$K_s$ (m/day)	$K_f$ (m/day)	RMSE
10	10.9	0.177
10	11.2	0.114
10	11.4	0.075
10	11.6	0.039
10	11.8	0.024
10	12	0.049

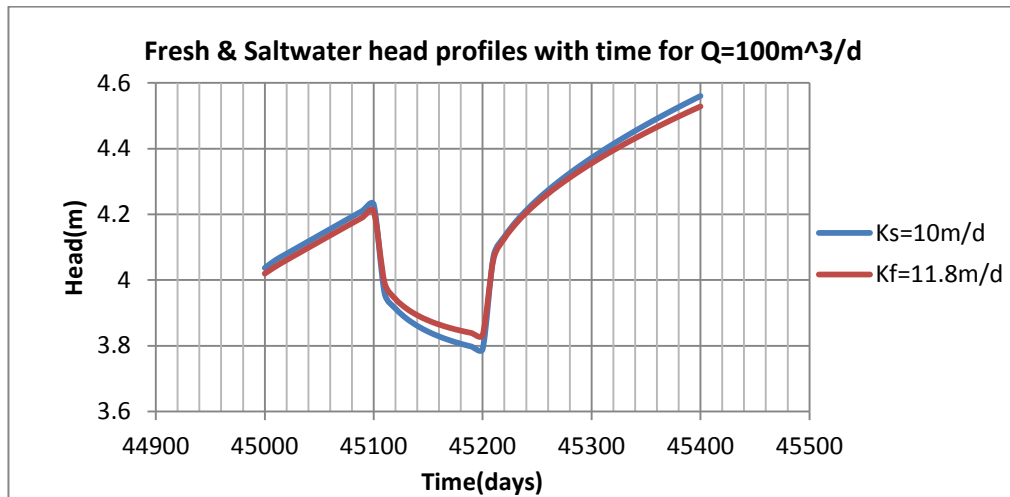


**Figure 5-3 Water table response comparison for (a) pumping scenario when  $K_s = 10$  m/day**

#### 5.2.2.2 Pumping Scenario (b)

For  $K_s$  equal 15 m/day the equivalent  $K_f$  value was 19 m/day. Table 5-6 illustrates the minimal RMSE determination among different  $K_f$  values and figure 5-4 shows a plot of the best fit between the two models.

**Table 5-6 Optimum  $K_f$  value determination for  $K_s= 15$  m/day**

$K_s$ (m/day)	$K_f$ (m/day)	RMSE
15	18.5	0.063
15	19	0.041
15	19.5	0.043
15	20	0.066

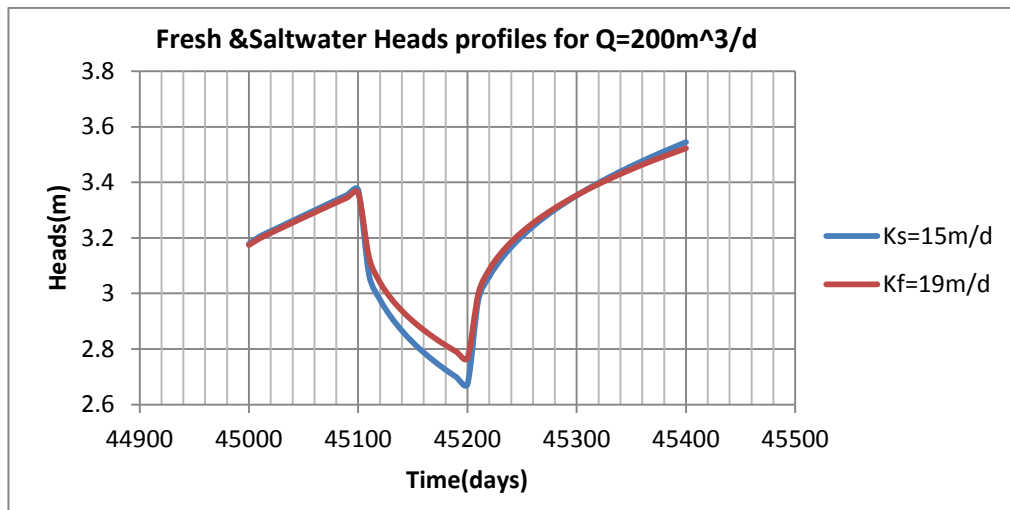


**Figure 5-4 Water table response comparison for (b) pumping scenario when  $K_s = 15$  m/day**

For  $K_s$  equal 20 m/day, the equivalent  $K_f$  was 28 m/day. Table 5-7 illustrates the minimal RMSE determination among different  $K_f$  values and figure 5-5 shows a plot of the best fit between the two models.

**Table 5-7 Optimum  $K_f$  value determination for  $K_s = 20$  m/day**

$K_s$ (m/day)	$K_f$ (m/day)	RMSE
20	27	0.054
20	28	0.041
20	29	0.053
20	30	0.076

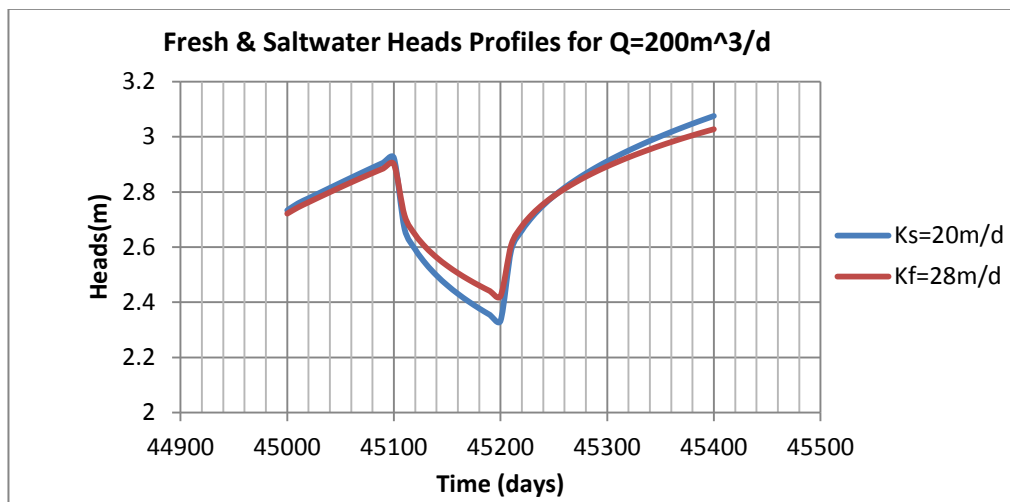


**Figure 5-5 Water table response comparison for (b) pumping scenario when  $K_s = 20$  m/day**

### 5.2.3 Second Simulation Set

The recharge rate ( $R$ ) was increased to 0.008 m/day. By increasing the recharge rate the average pure freshwater lens  $B_f$  increased from 50 m to 70 m. Different pumping rates were applied to obtain the same ratios of  $Q/B_f$  that we used in the first scenario. Five different pumping scenarios (f, g, h, i and j) were applied to the saltwater/freshwater model to generate five ratios for  $Q/B_f$ . Each pumping rate is applied to test the effect of saltwater presence for

different sand types within the full range of  $K_s$  ( $5 \text{ m/day} \leq K_s \leq 45 \text{ m/day}$ ). Table 5-8 summarizes the pumping amounts applied to the model, for the 5 desired  $Q/B_f$  ratios.

**Table 5-8 Ratios of  $Q/B_f$  for first simulation scenario**

<i>Recharge Rate</i> $R = m/day$	<i>Pumping rates</i> $Q = m^3/day$	<i>Approximate pure</i> <i>Freshwater lens (<math>B_f</math>)</i>	<i>(<math>Q/B_f</math>)</i> <i>Ratio</i>
$R = 0.008 \text{ m/day}$	f) 140	70 m	2
	g) 280		4
	h) 420		6
	i) 560		8
	j) 700		10

### 5.3 Compilation and Analysis of Results

The relationship between freshwater hydraulic conductivity  $K_f$  (m/day) and real hydraulic conductivity  $K_s$  (m/day) was plotted based on the normalized ratio of the pumping rate  $Q(m^3/day)$  over the pure freshwater lens  $B_f(m)$ . Figure 5-6 illustrates the general relationship between  $K_s$  and the equivalent  $K_f$  when the recharge rate is 0.005 m/day. The plots demonstrate the effect of intrusions on the aquifer behavior for different sand types.

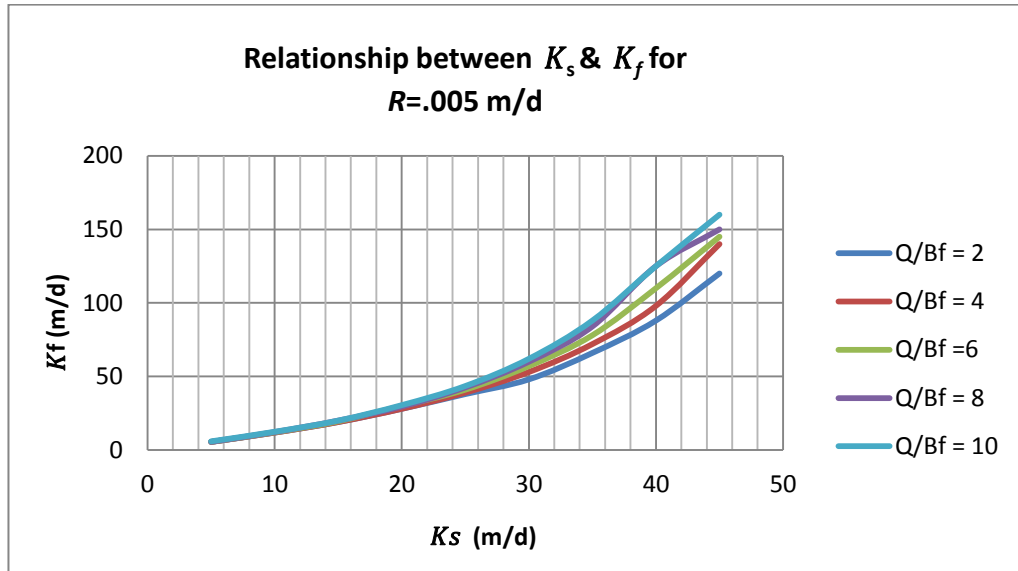


**Figure 5-6 General trend of the relationship between  $K_s$  and  $K_f$  for  $R=0.005$  m/day**

From the second simulation scenario, the general trend of the relationship between  $K_s$  and the equivalent  $K_f$  is the same as the first simulation set. Although the pure freshwater lens was thicker than in the first scenario, the effect of the intrusion on the aquifer behaviour was still pronounced. Figure 5-7 shows the general relationship between  $K_s$  and the equivalent  $K_f$  when the recharge rate is 0.008 m/day.

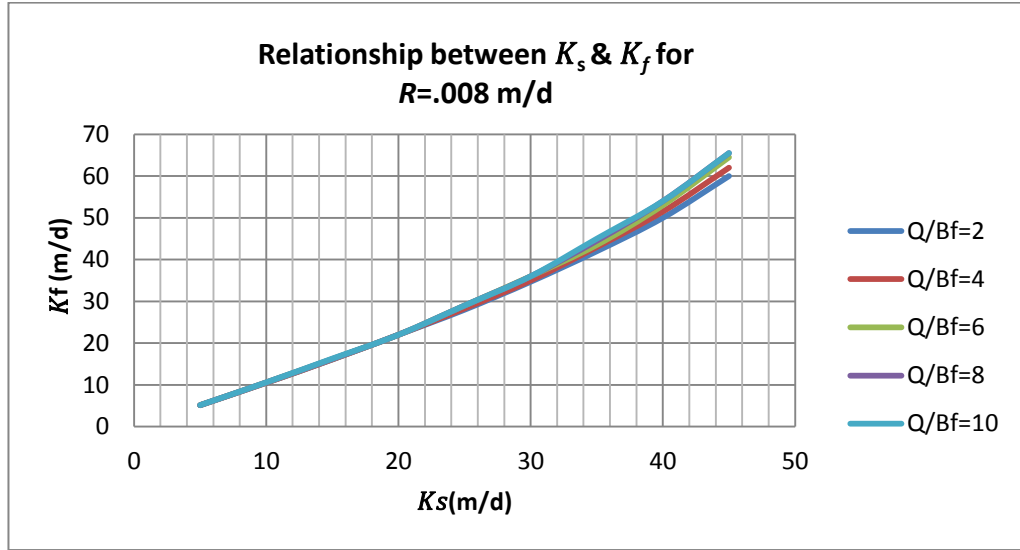


**Figure 5-7 General trend of the relationship between  $K_s$  and  $K_f$  for  $R=0.008$  m/d**

The quality of fit of the freshwater-only model (the RMSE achieved when comparing the 2D EFM to the 2D Saltwater/Freshwater model) is affected by the value of the aquifer hydraulic parameters ( $K_s$ ), and the ratio of  $Q/B_f$ . Figures 5-8 and 5-9 illustrate the relationship between  $Q/B_f$  versus the RMSE at different  $K_s$  values. The higher the aquifer conductivity becomes and the higher the pumping from a certain freshwater amount ( $B_f$ ), the poorer is the achievable fit between the freshwater-only model and the freshwater/saltwater models. In other words, the performance of the Equivalent Freshwater Model (EFM) deteriorates as the ratio  $Q/B_f$  increases and as the Hydraulic Conductivity of the aquifer increases. We can further see that the EFM works better, in general, as the thickness of the freshwater lens ( $B_f$ ) increases.



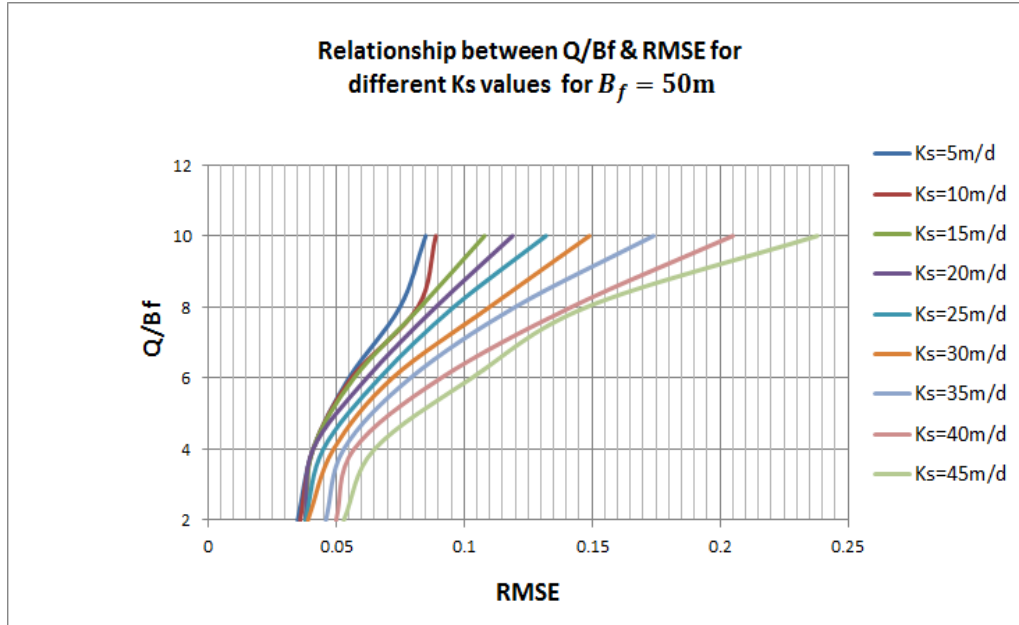


**Figure 5-8 Summary of the relationship between Q/B<sub>f</sub> and RMSE for B<sub>f</sub> = 50 m**

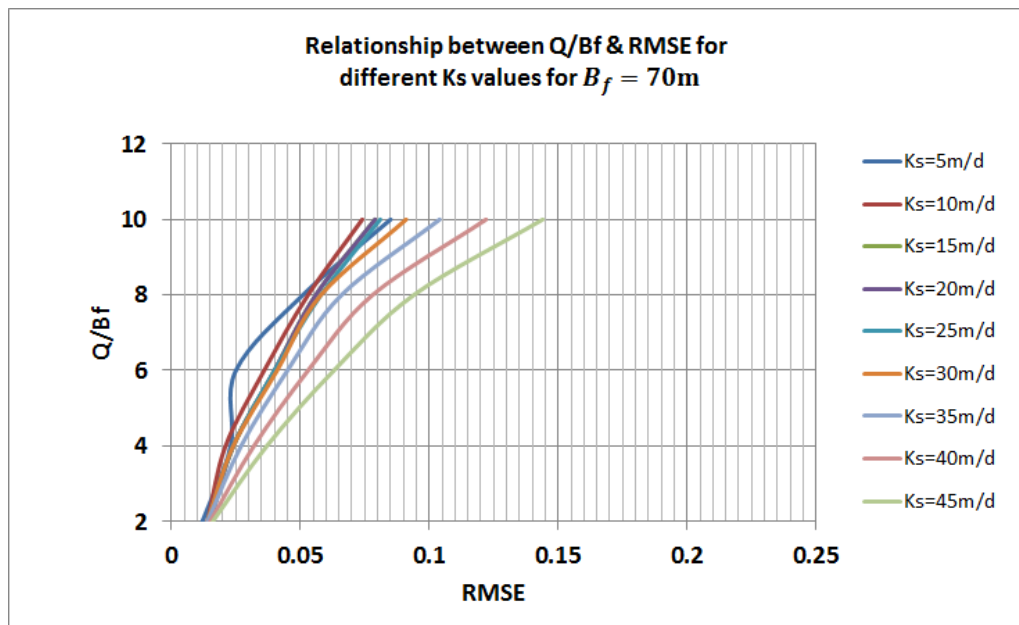


**Figure 5-9 Summary of the relationship between Q/B<sub>f</sub> and RMSE for B<sub>f</sub> = 70 m**

Although the RMSE is an appropriate tool to quantify the quality of any simulations, the examination of the error distribution is also important. Figures 5-10, 5-11 and 5-12 illustrate the error distributions for three simulations with different pumping scenarios that achieved the

same RMSE. We can see that the actual error is dependent on the pumping rate applied to the models; the higher the pumping, the higher the error. This shows that the performance of the Equivalent Freshwater model is poorer during the stress periods where pumping is applied and that the relationships between  $Q/B_f$  and RMSE presented above do not provide a complete picture of the performance of the EFM.

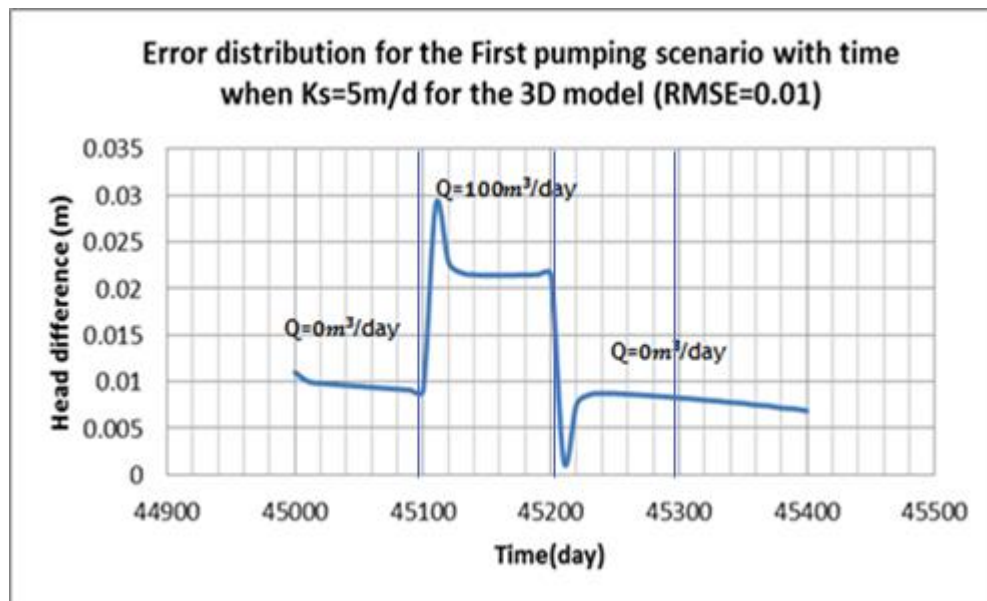


Figure 5-10 Difference in head distribution for the first pumping scenario for  $K_s = 5 \text{ m/day}$  and  $K_f = 5.5 \text{ m/day}$

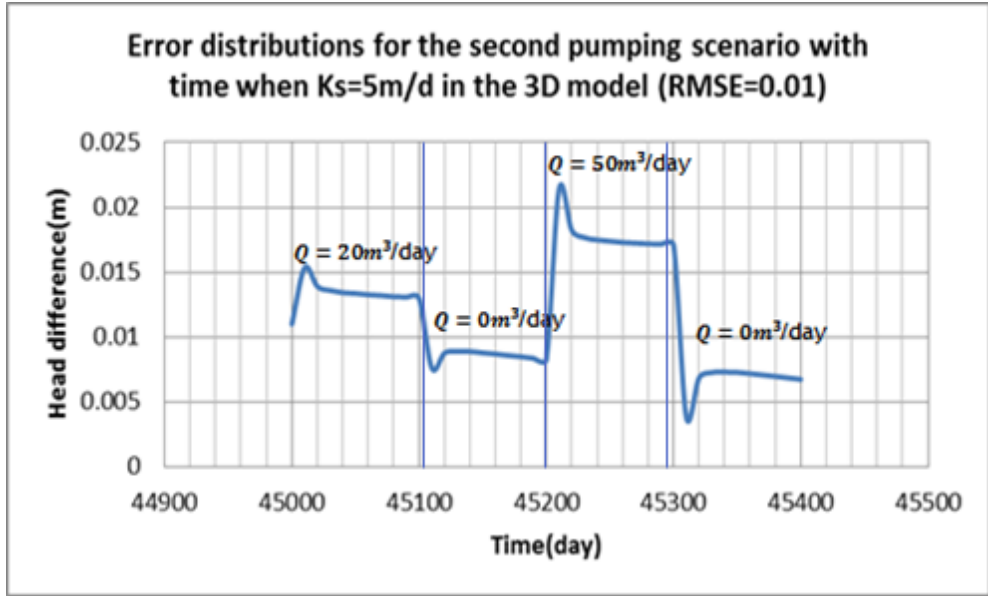


Figure 5-11 Difference in head distribution for the second pumping scenario for  $K_s = 5$  m/day and  $K_f = 5.5$  m/day

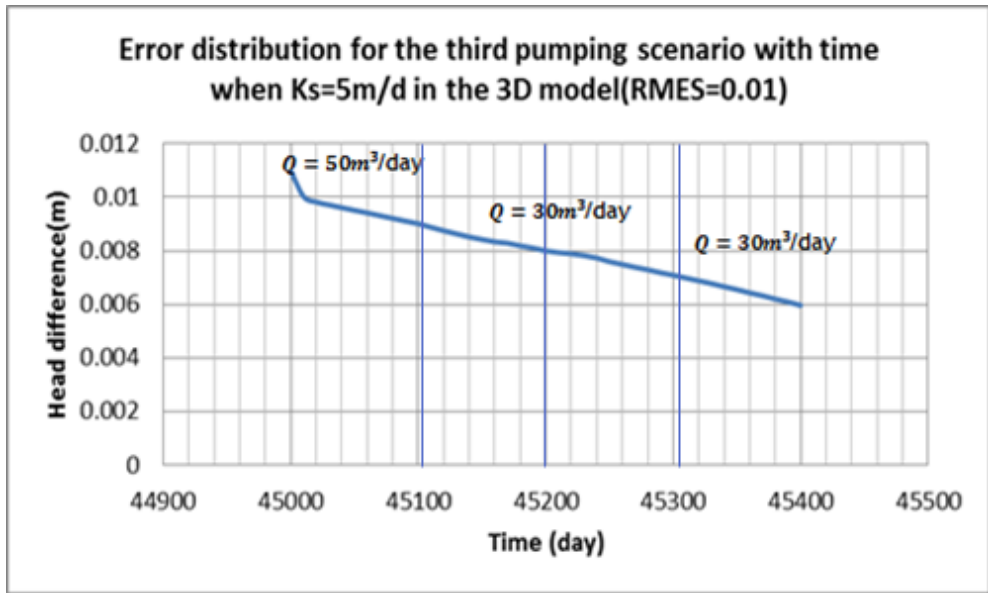


Figure 5-12 Difference in head distribution for the third pumping scenario for  $K_s = 5$  m/day and  $K_f = 5.5$  m/day

## Chapter 6

### Verification with Three-Dimensional Models

#### 6.1 Introduction

From 2D simulations, it was observed that the relationship between the real hydraulic conductivity ( $K_s$ ) and the equivalent freshwater hydraulic conductivity ( $K_f$ ) is almost linear for fine and medium sand soils, as shown in figures 6-1 and 6-2. The 3D model was created to test the validity of the previous relationships within hydraulic conductivity range of 5 m/day to 20 m/day for different pumping rates and pumping scenarios. Selected 2D  $K_f$  and  $K_s$  values have been used with saltwater/freshwater and freshwater-only 3D models and a comparison has been performed. Comparisons between the 2D RMSE values and the 3D RMSE values have also been done within the selected hydraulic conductivity range.

#### 6.2 Three Dimensional Saltwater Model Description

##### 6.2.1 Model Grid Description

The 3D model consists of 50 columns and 50 rows, with a cell size of 25 m by 25 m. The aquifer consists of 5 layers with a total thickness of 150m. The model top elevation is set at 9 m and the bottom elevation is set at 141 m below sea level. The layers thicknesses from the ground surface to the aquifer bottom are 30, 20, 20, 40 and 40 m respectively. According to the 2D model, when the recharge rate was 0.005 m/day the average corresponding freshwater thickness was 50 m. Based on what the 2D model gives, the 3D model layers thicknesses were set to represent the configuration of the freshwater, the transition zone and the brine

water thickness, as it was in the 2D model but with fewer layers. The first two layers are meant to include the freshwater lens, the third layer includes the transition between the freshwater and saltwater, while the last two layers include the pure saltwater. Figure 6-1 illustrates the 3D model dimensions.

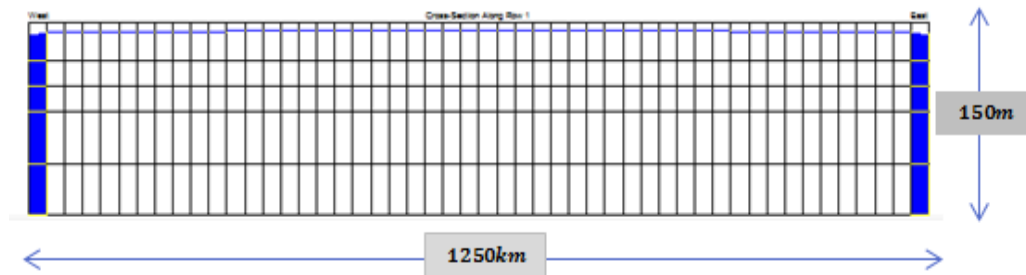


**Figure 6-1 3D model dimensions**

### **6.2.2 Model Hydrogeological Parameters**





Similar to the 2D model, the 3D generic saltwater/freshwater model is an unconfined homogenous and isotropic sand aquifer; the model hydraulic conductivity value is 20 m/day. The soil effective porosity is 0.28, the specific storage is 0.001, and the aquifer specific yield is 0.2. The aquifer longitudinal dispersivity was 2.5 m and the transverse dispersivity is 0.25 m. The initial salt concentration for the model is homogenous and equal to 35 kg/m<sup>3</sup>. The distribution factor  $K_d$  for the original saltwater chemical composition is 0.0086, and the diffusion coefficient was set at 0.001 m<sup>2</sup>/day.

### 6.2.3 Model Boundary Conditions

A uniform recharge was applied along the aquifer surface of 0.005m/day. A zero meter constant head boundary condition was applied along two opposite sides. The concentration at the boundary was constant and equal to 35 Kg/m<sup>3</sup>. A no flow boundary condition was set by default at the bottom of the aquifer. Two monitoring wells were installed, ( $M_1$ ) in the middle of the aquifer, at a distance  $X = 625\text{ m}$  and  $Y = 625\text{ m}$  while the other well ( $M'_s$ ) was at  $X = 625\text{ m}$  and  $Y = 225\text{ m}$ . Both wells were set in the first layer to measure the fluctuation in the water table and were also used as pumping wells. Another two wells, ( $M_2$ ) at  $x = 1000\text{ m}$ ,  $Y = 1000\text{ m}$  and ( $M_3$ ) at  $X = 250\text{ m}$  and  $Y = 1000\text{ m}$ , were used for pumping only.

The simulation was transient with a total time of approximately 124 years divided into five stress periods. The first stress period has been set to reach a steady state with a transient simulation. Then four stress periods of 100 day each, were used to introduce variable pumping. Table 6-1 summarizes the well locations and figure 6-2 illustrates the plan view of the 3D model.

**Table 6-1 Summary of types and positions of wells used in the 3D model**

Well number	Well distance in X direction	Well distance in Y direction	Well type
$M_1$ 	625 m	625 m	Pumping and monitoring
$M_2$ 	1000 m	1000 m	Pumping
$M_3$ 	250 m	1000 m	Pumping
$M'_s$ 	625 m	225 m	Pumping and monitoring

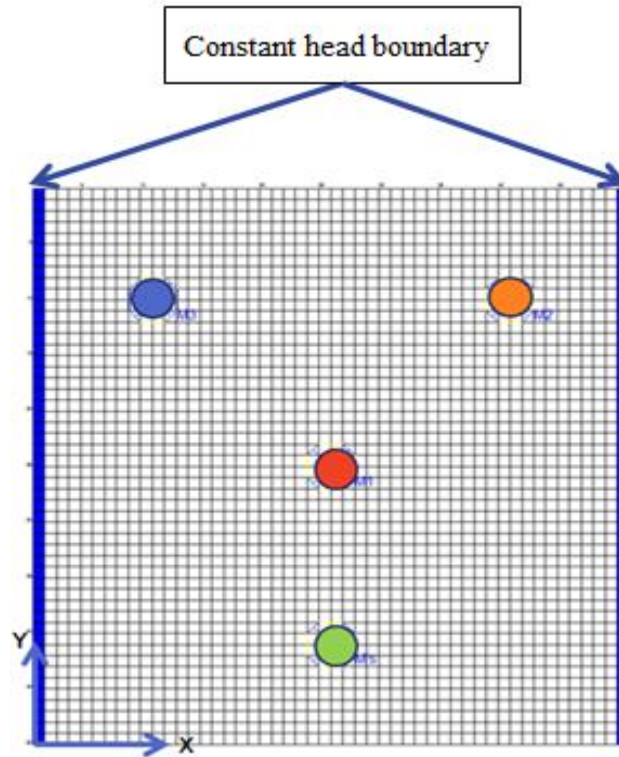


**Figure 6-2 Locations of pumping and monitoring wells**

#### **6.2.4 Model Numerical Flow and Transport Parameters**

The simulation was performed with SEAWAT, an implicit coupling approach was used and a finite difference solution scheme was applied. All simulation conditions were identical to those used for the 2D model. Table 6-2 and figure 6-3 both illustrate the 3D saltwater model parameters and elevation.

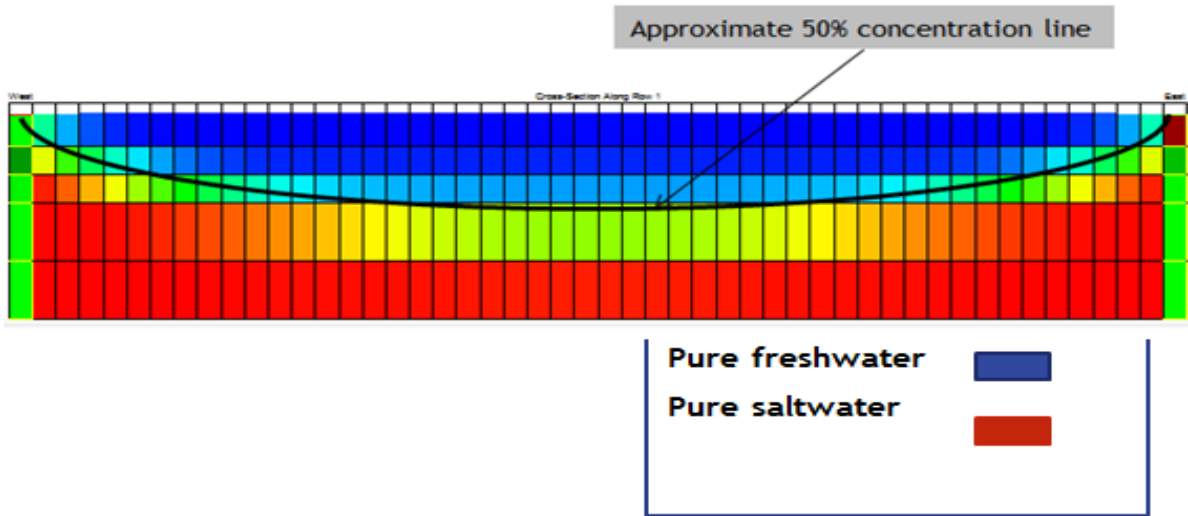


Figure 6-3 3D Saltwater generic aquifer model



**Table 6-2 Input and Numerical solution parameters for the saltwater generic aquifer model**

<b>Parameter</b>	<b>Value</b>
<b>Flow Parameters</b>	
$K_x=K_y=K_z$	20 m/day
$\theta$ effective porosity	0.28
$S_s$	0.001
$S_y$	0.2
$\alpha_l$	2.5 m
$\alpha_t$	0.25 m
D	0.001 m <sup>2</sup> /day
$C_{ini.}$	35 kg/m <sup>3</sup>
$K_d$	0.0086
R	0.005 m/day
$\rho_s$	1025 Kg/m <sup>3</sup>
$\rho_f$	1000 Kg/m <sup>3</sup>
<b>Numerical solution parameters</b>	
Cell size(coulmn1to50);dx,dz	25 X25 m
Cell size (row1 to 50); dx,dy	25 X25 m
<b>Solution of flow equation</b>	
Matrix solution technique	PCG
Head convergence value	1 X 10 <sup>-7</sup> m
Flow convergence value	1 X 10 <sup>-7</sup> kg/d
<b>Solution of transport equation</b>	
Advection term	Finite difference
Dispersion and source terms	Implicit finite difference ; GCG
Time-step length	10days
Courant number	Cr=1
Concentration convergence value	1 X 10 <sup>-6</sup>

### 6.2.5 3D Freshwater Model Description

The 3D freshwater model grid and parameters were identical to the saltwater version, except with respect to the Hydraulic Conductivity and the freshwater head boundary conditions. The freshwater head boundaries were created to match the 2D freshwater head model and to be equivalent to the 3D saltwater head boundary condition. The assigned heads were calculated using equation (24). The assigned equivalent freshwater boundary heads from top to bottom are, 0.15 m, 0.775 m, 1.275 m, 2.025 m and 3.025 m respectively.

## 6.3 Simulations and Pumping Sets for $R=0.005$ m/d

### 6.3.1 First Pumping Set

The created 3D model freshwater thickness with a recharge rate of  $R = .005$  m/d was equal to the fresh lens in the 2D model, which was 50 m. The first scenario applied a single pumping rate of 100 m<sup>3</sup>/day from well M<sub>1</sub>. Simulations of the saltwater/freshwater model were done with  $K_s$  values of 5, 10, 15, and 20 m/d. Corresponding simulations were performed with the freshwater-only model using the equivalent freshwater Hydraulic Conductivities  $K_f$  obtained previously from the 2D models. The different  $K_s$  values were divided into five groups (3D – a, 3D – b, 3D – c, 3D – d, and 3D – e) for each  $K_s$  value. Table 6-3 illustrates  $K_s$  values for the 3D model in the first simulation set and table 6-4 shows the comparison of the quality of fit obtained for each  $K_s$  and corresponding  $K_f$  values, in the 2D models and in the 3D models. Figures 6-4, 6-5, 6-6 and 6-7 show plots of the head profiles used to compute the RMSE for the 3D models. The blue curves show the saltwater/freshwater model response and the red curves show the freshwater-only model response.

**Table 6-3  $K_s$  values for the 3D model in the first simulation set**

<i>Model type</i>	<i>Recharge rate</i> <i>R (m/day)</i>	<i>First pumping Set</i>	<i>Tested <math>K_s</math> values</i>
Three dimensional model	$R = 0.005 \text{ m/day}$	$Q = 100 \text{ m}^3/\text{day}$	a) $K_s = 5 \text{ m/day}$
			b) $K_s = 10\text{m/day}$
			c) $K_s = 15\text{m/day}$
			d) $K_s = 20\text{m/day}$

**Table 6-4 Comparison between RMSE for 2D and 3D models**

$K_s$ (m/day)	$K_f$ (m/day)	2D RMSE	3D RMSE
5	5.5	0.03	0.01
10	11.8	0.02	0.06
15	19	0.03	0.09
20	28	0.03	0.20

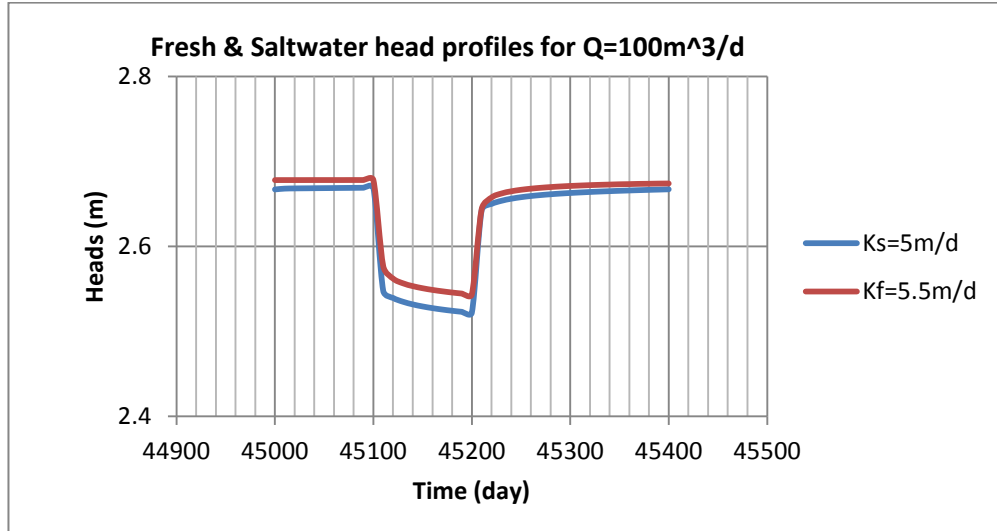


Figure 6-4 Head difference between  $K_s$  and  $K_f$  models for 3D- a' scenario

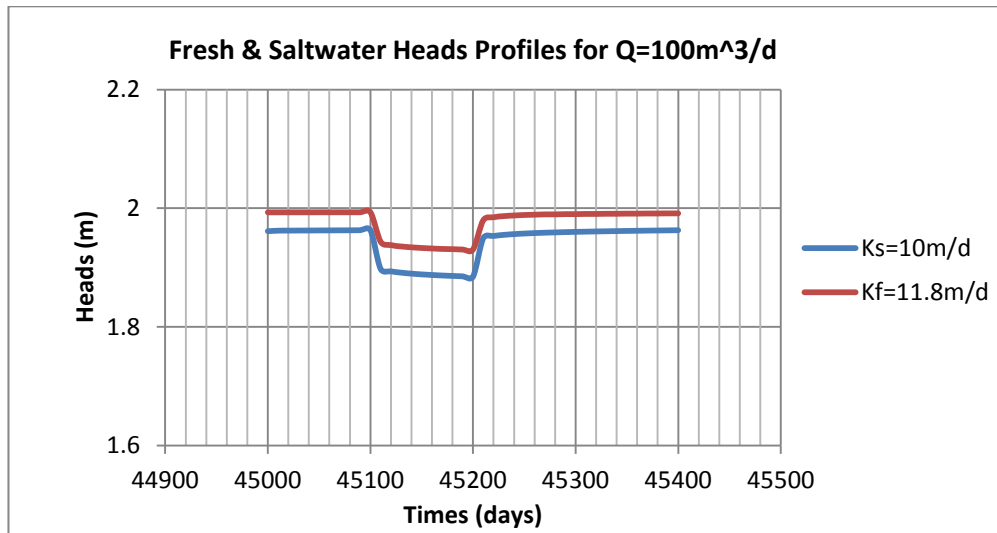


Figure 6-5 Head difference between  $K_s$  and  $K_f$  models for 3D- b' scenario

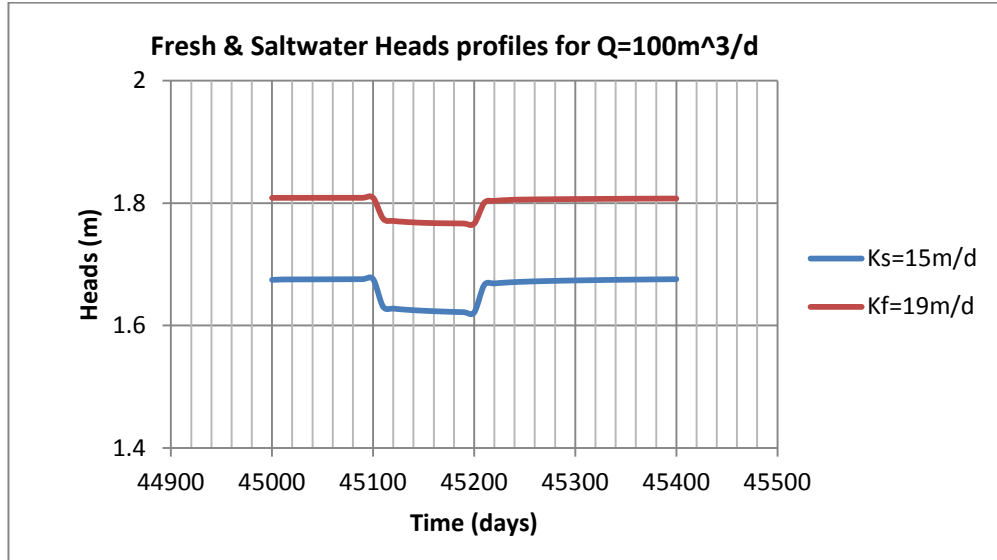


Figure 6-6 Head difference between  $K_s$  and  $K_f$  models for 3D- c' scenario

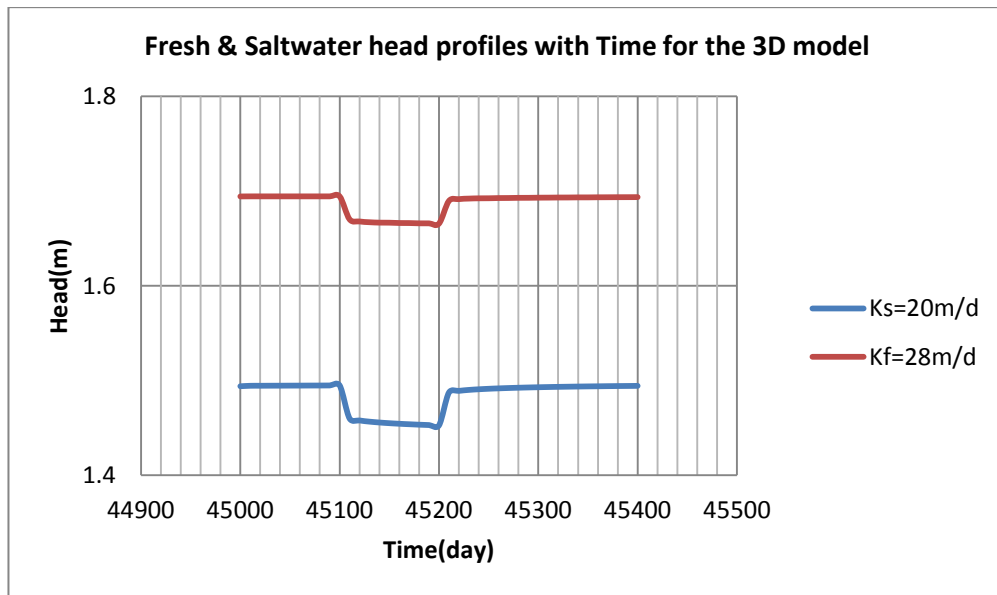


Figure 6-7 Head difference between  $K_s$  and  $K_f$  models for 3D- d' scenario

### 6.3.2 Second Pumping Set

The simulations were repeated in the second scenario; however, the pumping at well  $M_1$  has more than one pumping rate,  $20\text{ m}^3/\text{day}$  in stress period 2 and  $50\text{ m}^3/\text{day}$  in stress period 4.

The different  $K_s$  values were divided into five scenarios, like for the first pumping set. Table 6-5 illustrates the  $K_s$  values for the 3D model in the second simulation set. The RMSE values obtained were similar to the values that were obtained in the first scenario. Table 6-6 and figures 6-8, 6-9, 6-10 and 6-11 illustrate the results.

**Table 6-5  $K_s$  values for the 3D model in the first simulation set**

<i>Model type</i>	<i>Recharge rate R (m/day)</i>	<i>second pumping Set</i>	<i>Tested <math>K_s</math> values</i>
Three dimensional model	$R = 0.005 \text{ m/day}$	$Q = 20 \text{ m}^3/\text{day} \&$ $Q = 50 \text{ m}^3/\text{day}$	e) $K_s = 5 \text{ m/day}$
			f) $K_s = 10\text{m/day}$
			g) $K_s = 15\text{m/day}$
			h) $K_s = 20\text{m/day}$

**Table 6-6 Comparison between RMSE for 2D and 3D model**

$K_s$ (m/day)	$K_f$ (m/day)	2D(RMSE)	3D(RMSE)
5	5.5	0.03	0.01
10	11.8	0.02	0.06
15	19	0.03	0.08
20	28	0.03	0.20

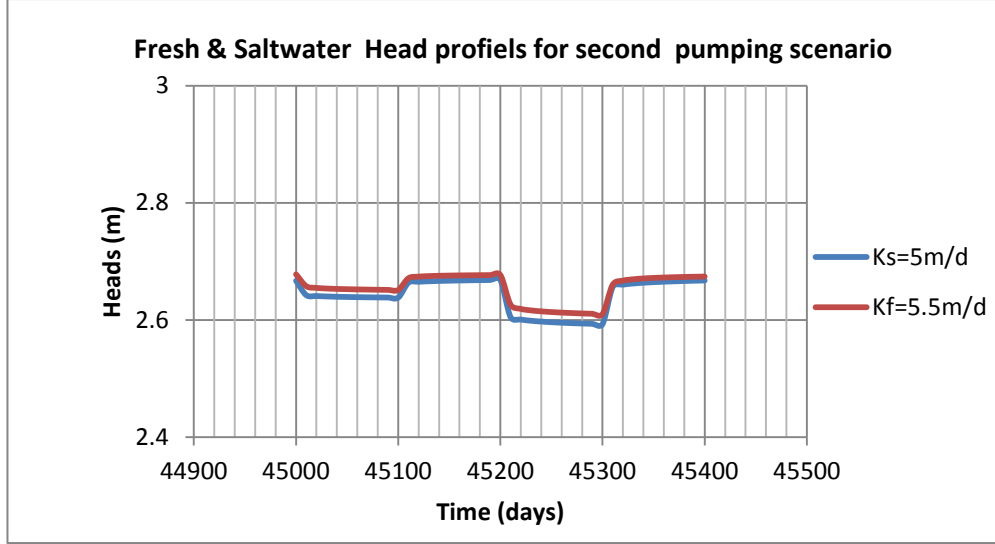


**Figure 6-8 Head difference between  $K_s$  and  $K_f$  models for 3D- e' scenario**

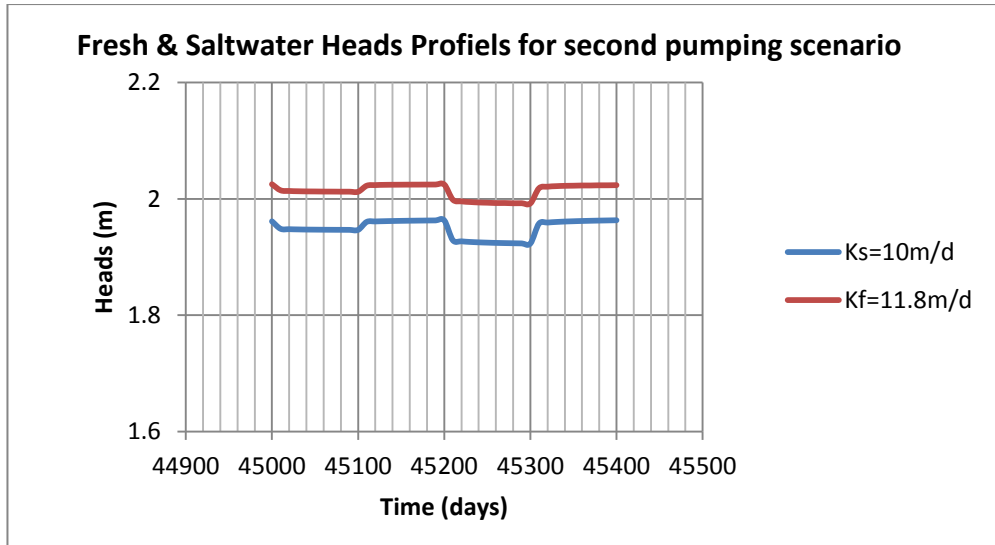


**Figure 6-9 Head difference between  $K_s$  and  $K_f$  models for 3D- f' scenario**

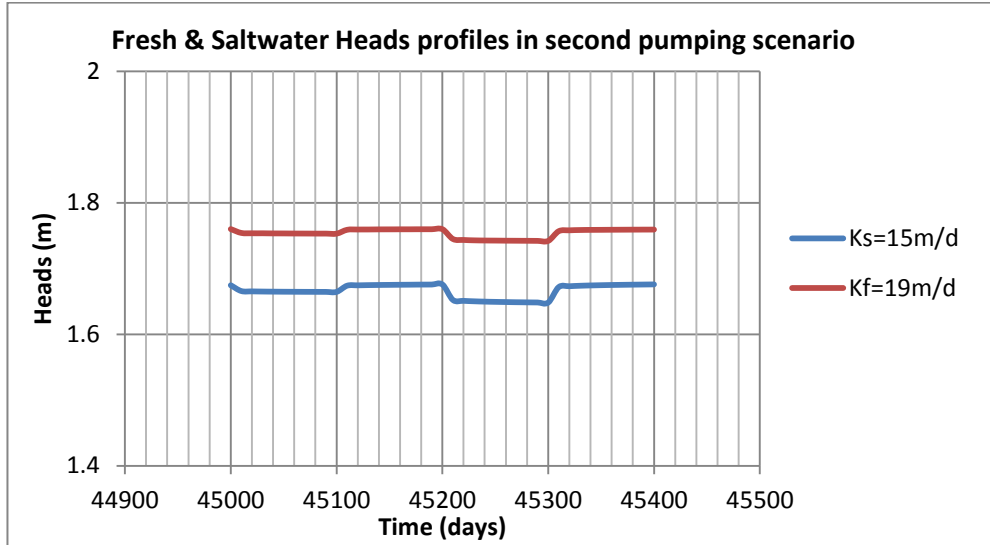


Figure 6-10 Head difference between  $K_s$  and  $K_f$  models for 3D- g' scenario

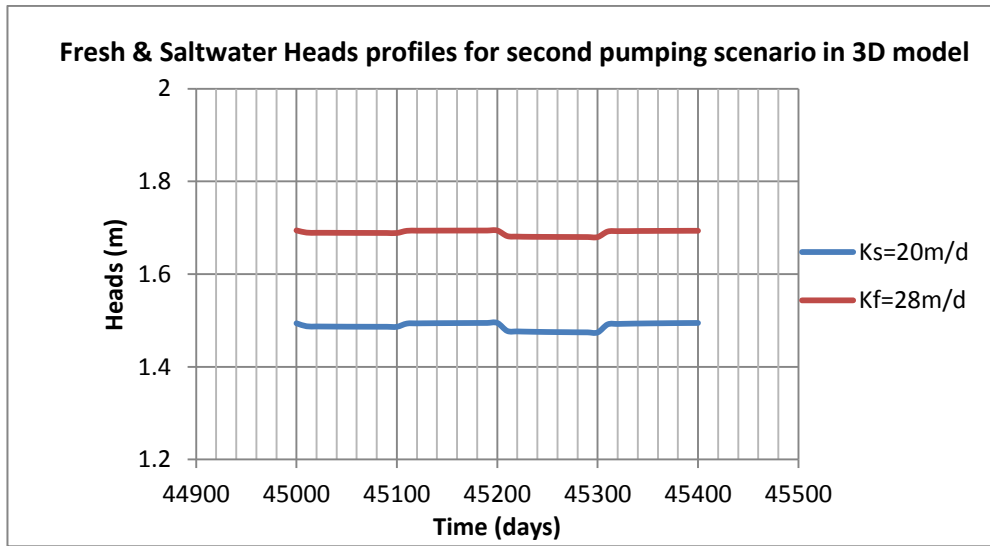


Figure 6-11 Head difference between  $K_s$  and  $K_f$  models for 3D- h' scenario

### 6.3.3 Third Pumping Set

In the third scenario, the pumping was applied at different wells, simultaneously. Wells  $M_1$ ,  $M_2$  and  $M_3$  were pumped at the same time with different pumping rates of 50, 30 and



30 m<sup>3</sup>/d, respectively and the head profiles have been recorded at well M<sub>s</sub>' . Different K<sub>s</sub> values were tested and divided into four groups. Table 6-8 illustrates K<sub>s</sub> values for the 3D model in the third simulation set. The results were K<sub>f</sub> again similar to the values obtained in the first two scenarios. Table 6-9 and figures 6-12, 6-13, 6-14 and 6-15 show the results.

**Table 6-7 K<sub>s</sub> values for the 3D model in the first simulation set**

<i>Model type</i>	<i>Recharge rate R (m/day)</i>	<i>Third pumping Set</i>	<i>Tested K<sub>s</sub> values</i>
Three dimensional model	R = 0.005 m/day	Q = 50 m <sup>3</sup> /day ,	i) K <sub>s</sub> = 5 m/day
		Q = 30 m <sup>3</sup> /day &	j) K <sub>s</sub> = 10 m/day
		Q = 30 m <sup>3</sup> /day	k) K <sub>s</sub> = 15 m/day
			l) K <sub>s</sub> = 20 m/day

**Table 6-8 Comparison between RMSE for 2D and 3D model**

K <sub>s</sub> (m/day)	K <sub>f</sub> (m/day)	2D(RMS)	3D(RMS)
5	5.5	0.03	0.01
10	11.8	0.02	0.06
15	19	0.03	0.08
20	28	0.03	0.20

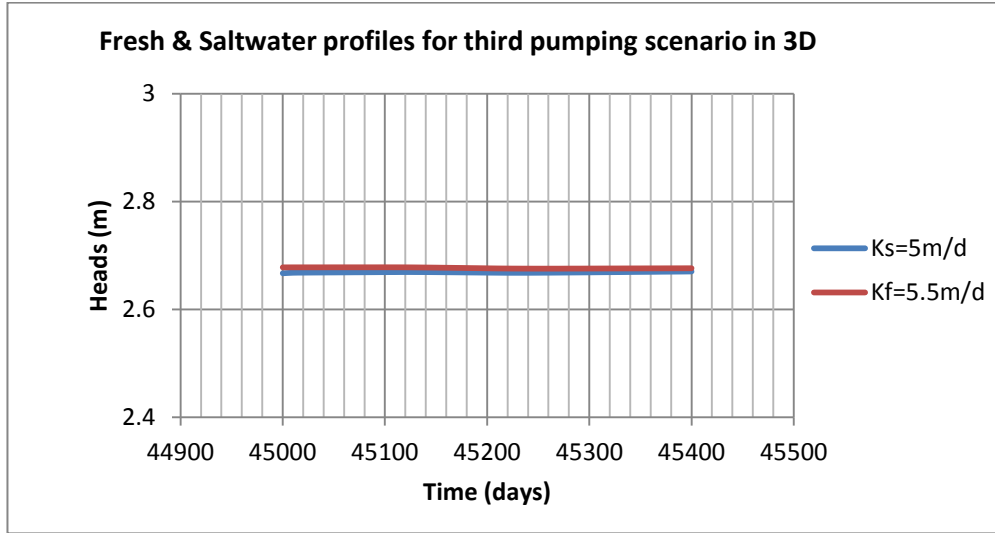


**Figure 6-12 Head difference between  $K_s$  and  $K_f$  for 3D-  $i'$  scenario**

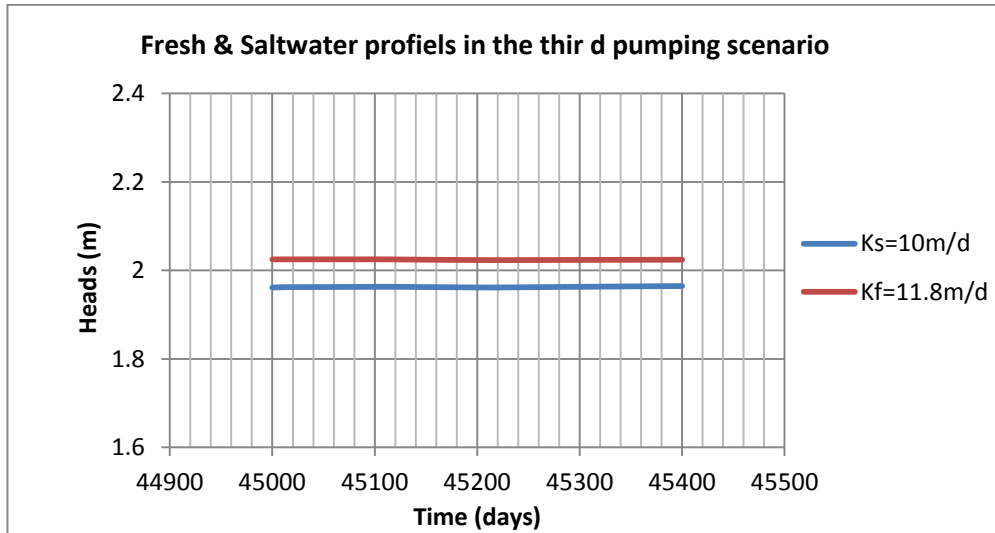


**Figure 6-13 Head difference between  $K_s$  and  $K_f$  for 3D-  $j'$  scenario**

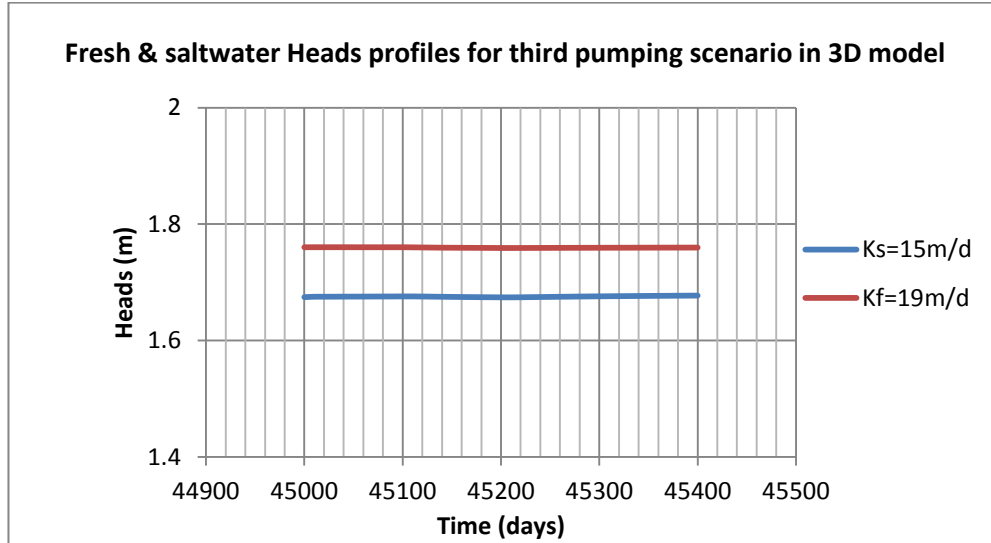


**Figure 6-14 Head difference between  $K_s$  and  $K_f$  for 3D-  $k'$  scenario**

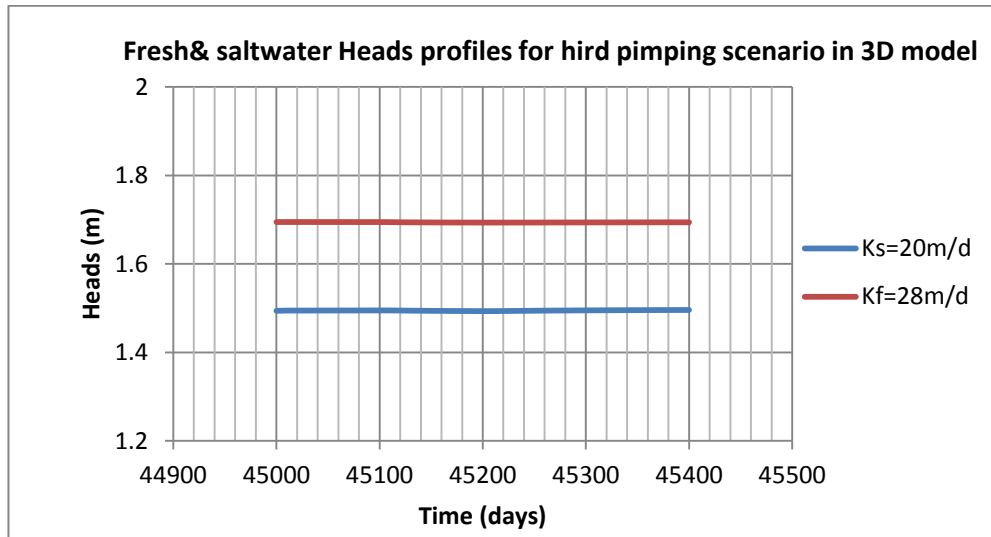


**Figure 6-15 Head difference between  $K_s$  and  $K_f$  for 3D-  $l'$  scenario**

## 6.4 Summary

In this chapter, a series of numerical simulations were presented in support of our study of the effect of a saltwater intrusion on an aquifer behavior. The developed 3D models,

saltwater/freshwater model and freshwater model, show that the aquifer behavior changes in the presence of a saltwater intrusion. For instance; in figures 6-4, 6-5, 6-6 and 6-7 it was found that the head difference between saltwater/freshwater only model and freshwater model starts small and is increased and decreased depending on the pumping rates. The head difference is distributed uniformly depending on the pumping rates. The 3D models verify the generated relationship between the aquifer real hydraulic conductivity  $K_s$  and the equivalent hydraulic conductivity  $K_f$  for different types of sand aquifers. In Chapter 7, the general conclusions and recommendations will be presented and discussed.

## Chapter 7

### Conclusions and Recommendations

#### 7.1 General

This research set out to test the hypothesis of the impact of the saline intrusion on the transient hydraulic behavior of coastal homogenous and isotropic sand aquifers. A two dimensional saltwater/freshwater model was developed and was investigated using SEAWAT. The model behavior was tested for different sand types, represented by different values of hydraulic conductivities, ranging from 5 m/day to 45 m/day. Another identical Equivalent Freshwater Model (EFM) was developed and investigated using MODFLOW. Equivalent freshwater hydraulic conductivities were produced as those values that yielded an equivalent behavior to the saltwater/freshwater model. The selected freshwater hydraulic conductivity values  $K_f$  were chosen based on the minimum RMSE. The simulations were run for different pumping and recharge rates. General relationships between  $K_s$  and  $K_f$  were produced, by normalizing each pumping rate values over the average pure freshwater lens ( $Q/B_f$ ). The selected equivalent freshwater hydraulic conductivity values have been tested and verified in a 3D saltwater/freshwater model under various pumping scenarios.

## 7.2 Conclusions

- 1) The results of the two dimensional and three dimensional simulations, demonstrate that the presence of saltwater influences the aquifer's transient hydraulic behavior and the significance of that impact depends on the aquifer's hydraulic conductivity.
- 2) In fine sand aquifers( $K_s \leq 5 \text{ m/day}$ ), the presence of saltwater intrusion does not significantly affect the aquifer behaviour, under the full range of pumping and freshwater lens thicknesses considered in this study. An Equivalent Freshwater Model using the natural hydraulic conductivity of the aquifer will adequately simulate the saltwater-encroached aquifer.
- 3) For medium sand aquifer( $K_s \leq 20 \text{ m/day}$ ), the presence of the intrusion requires an Equivalent Freshwater Hydraulic Conductivity ( $K_f$ ) that is 20 to 30% higher than the original value, but the required  $K_f$  is fairly independent of the pumping over the freshwater lens thickness ratio ( $Q/B_f$ ). An EFM using a ( $K_f$ ) value that is 20 to 30% higher than the natural hydraulic conductivity will adequately simulate a wide range of pumping and recharge scenarios.
- 4) For coarse sand aquifers( $K_s \leq 45 \text{ m/day}$ ); the saltwater presence does have a significant effect on the aquifer behaviour and the ratio of  $K_f$  over  $K_s$  is significantly affected by the freshwater lens thickness, as well as the pumping. In this case an EFM may not be effective, since the required  $K_f$  values are dependent on the aquifer properties and stresses and therefore are not readily available.

- 5) In fine and medium sand aquifers, there is no need to use a variable-density simulation code to predict the response of the freshwater component, as a freshwater-only model, using an appropriate Equivalent freshwater Hydraulic Conductivity, will adequately simulate the behaviour of the aquifer.

### **7.3 Recommendations and Future Work**

1. More investigations are needed to establish the effect of saline intrusion on the transient hydraulic behaviour for coarse sand aquifers.
2. Developing a general relationship between  $K_s$  and  $K_f$  for coarse sand aquifers is a logical next step of this research program.
3. The effect of saltwater encroachment on the transient hydraulic behaviour for non-homogeneous anisotropic sand aquifers should be investigated.
4. The importance of anisotropic ratios on coastal aquifers should be investigated.

## References

**Abd-Elhamid, H. and A., Javadi, (2011)**, A density-dependant finite element model for analysis of saltwater intrusion in coastal aquifers, *Journal of Hydrology*, 401.

**Abdel-Mohsen, S.S, M., Tetreault, and M.E., Hulley, (2013)**, Saltwater Intrusion in Coastal Aquifers. 48th Eastern Canadian Symposium on Water Quality Research, Canadian Association on Water Quality. Kingston, ON, Canada.

**Abdel-Mohsen, S.S, M., Tetreault, and M.E., Hulley, (2014)**, An Equivalent Freshwater Modelling Approach for Coastal Aquifer, Civil Engineering Research Report CE-2014-1 Royal Military College of Canada.

**Aharmouch, A. and A., Larabi, ( 2001)**, Numerical Modeling of Saltwater Interface Up-coning Coastal aquifers, First International Conference on Saltwater Intrusion and Coastal Aquifers Monitoring, Modeling, and Management.

**Bear, J. (1972)**, Dynamics of Fluids in porous Media, Dover Publication, Inc., New York.

**Bear, J. and G., Dagan, (1964)**, The Unsteady Interface below a Coastal Collector, The Transition Zone between Fresh and Saltwater in a Coastal Aquifer. Report 3, Technion, Haifa, Israel, IASH.



**Chow, V.T., (1964)**, Handbook of applied hydrology, McGraw Hill Book Company, New York, N.Y.

**Cooper, H.H, (1964)**, A Hypothesis Concerning the Dynamic Balance of Fresh Water and Salt Water in a Coastal Aquifer , Sea Water in Coastal Aquifers, U. S. Geological Survey.

**Dagan, G., (1971)**, Motion of Seawater Interface in Costal Aquifers, Water Recourse Research, 7 (3).

**Dagan, G., (1987)**, Theory of Solute Transport by Groundwater, Department of Fluid Mechanics and Heat Transfer, Faculty of Engineering, Tel Aviv University.

**DHI-WASY, (2010)**, FEFLOW, Finite Element subsurface Flow and Transport Simulation System. Berlin, Germany, Institute of water Resources Planning and Systems Research. 2.

**DHI-WASY GmbH Group, (2005)**, FEFLOW. Finite Element Subsurface Flow and Transport Simulation System, Berlin, Germany, WASY, Institute for water Resources Planning and System Research. 2.

**Elder, J.W., (1967)**, Transient convection in a porous medium: Journal of Fluid Mechanics, 27 (3).

**Faust, C.R., L.S., Sims, C.P., Spalding, P.F., Andersen and D.E., Stephenson, (1990),** FTWORK, A Three-Dimensional Groundwater Flow and Solute Transport Code, Westinghouse Savannah River Company.

**Fetter, C.W., (2001),** Applied Hydrogeology, Prentice-Hall, Inc., U.S.A.

**Glover, R.E., (1959),** The Pattern of Fresh-Water Flow in a Coastal Aquifer, Journal of Geophysical Research, 64 (4).

**Healy, H.G. and R.W., (1990),** Simulation of solute Transport in Variably Saturated Porous Media with supplemental information of modification, U.S. Geological Survey.

**Henry, H.R., (1964),** Interfaces between Salt Water and Fresh Water in Coastal Aquifers, Sea Water in Coastal Aquifers, U. S. Geological Survey.

**Henry, H.R., (1964),** Effects of Dispersion on Salt Encroachment in Coastal Aquifers, Sea Water in Coastal Aquifers, U. S. Geological Survey.

**Krieger, R.A., J.L., Hatchett and J.L., Poole, (1957),** Preliminary survey of the saline water resources of the United States, U.S. Geological Survey.

**Kohout, F.A., (1960),** Cyclic Flow of Salt Water in the Biscayne Aquifer of Southeastern Florida, Journal of Geophysical Research, 65 (7).

**Konikow, L. K., W. E., Sanford, and P. J., Campbell, (1997).** Constant concentration boundary condition: Lessons from the HYDROCOIN variable-density ground water benchmark problem, *Water Resource Research*, 33 (10).

**Langevin, C.D., and W., Guo, (2006),** MODFLOW/MT3DMS–Based Simulation of Variable-Density Ground Water Flow and Transport, *Groundwater*, 44 (3).

**Langevin, C.D. and W., Guo, (1999),** Improvements to SEAWAT, a variable-density modeling code [abs.], *EOSTransactions*, 80 (46).

**Lin, H.J., G.T., Yeh and J.R., Cheng, (1997),** FEMWATER, A Three dimensional Finite Element Computer Model for Simulating Density Dependent Flow and Transport in Variably Saturated Media, U.S.Army Engineer waterway Experiment station.

**Mercado, A., (1985),** The use of Hydro geochemical patterns in Carbonate Sand and Sand Stone Aquifers to Identify Intrusion and Flushing of Saline Water. *Groundwater*, 23 (5).

**Reilly, T.E., and Goodman, A.S., (1985),** Quantitative Analysis of Saltwater-Freshwater Relationship in Groundwater Systems- a Historical Perspective, *Journal of Hydrology*, 80.

**Reilly, T.E., and Goodman, A.S., (1987),** Analysis of Saltwater Up-coning Beneath a Pumping Well, *Journal of Hydrology*, 89.

**Strack, O. L.D., (1971),** Some Cases of Interface Flow towards Drains, Journal of Engineering Mathematics, 6 (2).

**Schmorak, S. and Mercado, A., (1969),** Up-coning freshwater interface below pumping well, field study, Water Resource Research, 5 (6).

**Simpson, M.J. and Clement, T.P., (2003),** Theoretical analysis of the worthiness of Henry and Elder problems as benchmarks of density-dependent groundwater flow models, Advances in Water Resources, 26.

**Siarkos, I. and Latianopoulos, D., (2012),** *Delineation of Wellhead Protection Zones for the control of point Pollution Sources in the aquifer of N.Moudania, Greece, European Water, 40.*

**Tain Shing, M.a., Marios, S., Yun-Sheng Yu, and R. W. Buddemeier, (1997),** Modeling Saltwater up-coning in a freshwater aquifer in south-central Kansas, Journal of Hydrology, 201.

**Todd, D.K., and Mays, L.W., (2011),** Groundwater Hydrology. John Wiley and Sons Inc., U.S.A.

**Tétreault, M.M., and Hulley, ME., (2011),** A Regional-Scale Groundwater Model of Barbados, MODFLOW and More 2011: Integrated Hydrologic Modeling - Conference

Proceedings, Maxwell, Poeter, Hill, & Zheng Eds. June 2011, Colorado School of Mines, igwmc.mines.edu.

**U.S Geological Survey, (2010)**, Saturated- Unsaturated Variable -Density Ground-Water Flow with Solute or Energy Transport (SUTRA), U.S Geological Survey, 2.2.

**U.S Geological Survey, (2002)**, A Computer program for simulation of three-dimensional Variable-density ground-water flow, U.S Geological Survey book 6.

**Van der veer, P., (1977)**, Analytical Solution for a Two-fluid Flow in a Coastal Aquifer Involving a Phreatic Surface with Precipitation. *Journal of Hydrology*, 35.

**Van Dam, J.C., (1983)**, The shape and position of the salt water wedge in coastal aquifers. *Relation of Groundwater Quantity and Quality*, 146.

**Voss, C.I., and Souza, W.R., (1987)**. Variable density flow and solute transport simulation of regional aquifers containing a narrow freshwater-saltwater transition zone. *Water Resource Research*, 23(10).

**Zheng, C., and Bennett, G.D., (2002)**, *Applied Contaminant Transport Modeling*. John Wiley & Sons, Inc., Publication, New York.